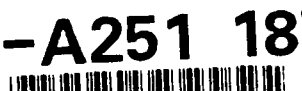

OFFICE OF NAVAL RESEARCH

Contract N00014-90-J-1159
R&T Code 413n007

Technical Report No. 9

Class B Sodalites: Nonstoichiometric Silver, Sodium Halosodalites

by

A. Stein, G.A. Ozin and G.D. Stucky

Prepared for Publication in

Journal of the American Chemical Society

May 15, 1992

REPORT DOCUMENTATION PAGE

Form Approved
OMB No. 0704-0188

1. AGENCY USE ONLY (Leave blank)	2. REPORT DATE	3. REPORT TYPE AND DATES COVERED
	05-15-92	Technical 06-01-91 to 05-31-92

4. TITLE AND SUBTITLE
Class B Sodalites: Nonstoichiometric Silver, Sodium Halosodalites

5. FUNDING NUMBERS
N00014-90-J-1159

6. AUTHOR(S)
A. Stein, G.A. Ozin, and G.D. Stucky

7. PERFORMING ORGANIZATION NAME(S) AND ADDRESS(ES)
University of California
Department of Chemistry
Santa Barbara, CA 93106

8. PERFORMING ORGANIZATION REPORT NUMBER
T9

9. SPONSORING/MONITORING AGENCY NAME(S) AND ADDRESS(ES)
Office of Naval Research
Chemistry Program
800 N. Quincy Street
Alexandria, VA 22217

10. SPONSORING/MONITORING AGENCY REPORT NUMBER

11. SUPPLEMENTARY NOTES
Prepared for Publication in the Journal of the American Chemical Society

12a. DISTRIBUTION/AVAILABILITY STATEMENT
Approved for public release;
distribution unlimited

12b. DISTRIBUTION CODE

13. ABSTRACT (Maximum 200 words)

Nonstoichiometric silver, sodium bromosodalites of the compositions $M_{8-2n}N_{2n}X_{2-p}OH_p$-SOD and $M_{8-p-2n}N_{2n}X_{2-p}[]_p$-SOD have been synthesized, where M, N = Ag^+, Na^+; X = Cl^-; Br^-, I^-; 2n = 0-8; p = 0-2; [] refers to anion-free cages and SOD = $(SiAlO_4)_6^{6-}$. These materials allow one to control the filling of both Ag^+ and X^- ions in a sodalite host lattice in a systematic manner, to fabricate $Na_{4-n}Ag_nX$ semiconductor-component clusters. Combined results from powder XRD, Rietveld refinement, ^{23}Na MAS and DOR NMR, far-IR and mid-IR indicate that these sodalites form a solid solution of $Na_{3-m}Ag_m$ clusters in anion-free ß-cages interspersed with $Na_{4-n}Ag_nX$. The clusters are statistically distributed throughout the lattice. However, silver ions are associated preferentially with cavities containing halide anions. The data also demonstrate that these materials offer the opportunity to manipulate the extent of collective electronic and vibrational interactions between monodispersed $Na_{4-n}Ag_nBr$ clusters in a perfectly crystalline host. The anion strongly mediates the vibrational coupling. The electronic coupling between clusters increases with Ag^+ and X^- loading level. Support for this idea comes from extended Hückel molecular orbital calculations. At low Ag^+/X^- loadings, intrasodalite AgX resembles the gas phase molecule (bond length, optical spectra). Optical absorption bands broaden and the absorption edge moves towards that of the bulk semiconductor at higher Ag^+/X^- loadings.

14. SUBJECT TERMS	15. NUMBER OF PAGES
	45
	16. PRICE CODE

17. SECURITY CLASSIFICATION OF REPORT	18. SECURITY CLASSIFICATION OF THIS PAGE	19. SECURITY CLASSIFICATION OF ABSTRACT	20. LIMITATION OF ABSTRACT
Unclassified	Unclassified	Unclassified	UL

Class B Sodalites: Nonstoichiometric Silver, Sodium Halosodalites

Andreas Stein, Geoffrey A. Ozin*

Lash Miller Chemical Laboratories, University of Toronto, 80 St. George St., Toronto, Ontario, Canada, M5S 1A1.

Galen D. Stucky

Department of Chemistry, University of California, Santa Barbara, California, U. S. A., 93106

Abstract

Nonstoichiometric silver, sodium bromosodalites of the compositions $M_{8-2n}N_{2n}X_{2-p}OH_p$-SOD and $M_{8-p-2n}N_{2n}X_{2-p}[]_p$-SOD have been synthesized, where M, N = Ag^+, Na^+; X = Cl^-, Br^-, I^-; 2n = 0-8; p = 0-2; [] refers to anion-free cages and SOD = $(SiAlO_4)_6^{6-}$. These materials allow one to control the filling of both Ag^+ and X^- ions in a sodalite host lattice in a systematic manner, to fabricate $Na_{4-n}Ag_nX$ semiconductor-component clusters. Combined results from powder XRD, Rietveld refinement, ^{23}Na MAS and DOR NMR, far-IR and mid-IR indicate that these sodalites form a solid solution of $Na_{3-m}Ag_m$ clusters in anion-free β-cages interspersed with $Na_{4-n}Ag_nX$ clusters. The clusters are statistically distributed throughout the lattice. However, silver ions are asssociated preferentially with cavities containing halide anions. The data also demonstrate that these materials offer the opportunity to manipulate the extent of collective electronic and vibrational interactions between monodispersed $Na_{4-n}Ag_nBr$ clusters in a perfectly crystalline host. The anion strongly mediates the vibrational coupling. The electronic coupling between clusters increases with Ag^+ and X^- loading level. Support for this idea comes from extended Hückel molecular orbital calculations. At low Ag^+/X^- loadings, intrasodalite AgX resembles the gas phase molecule (bond length, optical spectra). Optical absorption bands broaden and the absorption edge moves towards that of the bulk semiconductor at higher Ag^+/X^- loadings.

To be submitted as a Paper to the Journal of the American Chemical Society.

Introduction

Recently we have shown[1,2] that Class A silver, sodium halosodalites allow the atomically precise assembly of I-VII semiconductor components in a sodalite lattice. By tuning the silver concentration it was possible to cover the range from silver bromide exhibiting molecular behavior at low silver loadings to an expanded silver bromide supralattice at complete silver exchange[1]. In this paper a series of novel silver, sodium halo, hydrosodalites of the type $Na_{8-p-2n}Ag_{2n}X_{2-p}[]_p$-SOD, where SOD = $Si_6Al_6O_{24}$, [] = an anion free cage, p = 0-2, 2n = 0-8, will be discussed, which are derived from $Na_8X_{2-p}(OH)_p$-sodalites[3]. In these materials single size $Na_{4-n}Ag_nX$ (n = 0-4) clusters are dispersed within a perfectly periodic array of all-space filling β-cages, but in contrast to the previously described sodalites (Class A, Class C)[1,2,4], they are isolated from each other by sodalite cages containing no anion, forming a Class B supralattice of non-stoichiometric[5] silver, sodium halosodalite. The anion-free cages are filled with $Na_{3-n}Ag_n$ (n = 0-3) triangles, and in the hydrated form, with water molecules. Denks[5] has defined a nonstoichiometric sodalite as a solid-phase solution of NaX-SOD and Na[]-SOD, in which overall β-cavities with sodalitic and zeolitic fillings are statistically interspersed. Our definition of Class B sodalites also includes sodalites containing non-stoichiometric amounts of other anions, including the oxalates[6] and the halates recently prepared by Hund and Geismar ($Na_8X_{2-p}(OH)_p$-SOD, X = ClO_3, BrO_3, ClO_4)[7], as well as their silver derivatives. The endmembers for p=2, non-basic hydrosodalite (Na[]-SOD), hydroxosodalite (NaOH-SOD, basic hydrosodalite) are considered in this paper as special cases of Class B sodalites. The other endmembers of the series with p = 0 are really Class A sodalites. The hydrated forms of Class B sodalites contain additional water molecules, *e.g.*, zeolite Zh = Na[]-SOD, up to four water molecules per β-cage, and NaOH-SOD one water molecule per cavity[8] (up to two water molecules according to Ernst *et al.* and Felsche *et al.* [9,10] and up to three according to Denks[5]). As water can pass through the sodalite six-rings, these framework aluminosilicates can be classified as zeolites[5].

For Class A sodalites it has been shown[2], that orbital overlap and electronic/vibrational communication is possible between clusters in adjacent cages and therefore throughout the lattice. In Class B sodalites on the other hand, cages lacking an anion break the periodicity

between Ag_4X^{3+} clusters. This effect can change co-operative effects between clusters, which require the presence of a halide atom (vibrational) or its orbitals (electronic). For a solid solution, variations in the halide content, p, are expected to alter the mean distance between $Na_{4-n}Ag_nX$ clusters while changes in the silver content, n, and thus the sodium:silver ratio, shift the constituents of the clusters from those of an insulator to a semiconductor type. At low halide and silver concentrations isolated AgX molecules may be produced in Class B materials. Such controlled tunable volume filling and compositional alteration of the contents of the sodalite β-cages provides an unprecedented opportunity to adjust the extent of electronic and vibrational coupling between fixed nuclearity $Na_{4-n}Ag_nX$ clusters. It should therefore be possible to chemically manipulate the electronic band structure of the materials, and thus their electronic and optical properties. The synthetic details and structural, vibrational, magnetic resonance and optical properties of the Class B sodalites will be addressed in this paper.

Synthesis

Synthesis of Sodium Sodalite Precursors

The sodium sodalites were prepared by a low temperature hydrothermal synthesis. The gel compositions are listed in Table 1 and the reagent sources in Table 2. In a typical synthesis, solution A contained the sodium salt, sodium hydroxide and silica source and solution B contained sodium hydroxide and the alumina source. These were prepared as follows. For solution A, $0.6 \cdot z$ moles of NaOH and w moles of the sodium salt to be occluded in the sodalite were dissolved in $0.6 \cdot v$ moles of deionized water. An aqueous colloidal silica solution containing y moles of SiO_2 was added to the above solution. The solution was mixed and heated to 80-95°C. Solution B was prepared by dissolving x moles of $Al(OH)_3$ in an aqueous solution containing $0.4 \cdot z$ moles of the NaOH, again at 80-95°C. The hot solutions A and B were mixed rapidly. A gel formed almost immediately upon mixing. The gel was shaken for 5 minutes and the mixture was heated at 95°C for 3 - 9 days in 1000 mL capped teflon (FEP) bottles. The white, microcrystalline products were filtered through ASTM 10-15 medium pore glass frits and washed with 2-4 L deionized water. The products were dried in air at ambient temperature.

Soxhlet Extraction

Sodium hydroxosodalites and sodalites containing hydroxide in addition to halide anions were Soxhlet extracted to remove one NaOH molecule per cage. The hydroxide ion is the only anion small enough to pass through the sodalite six-rings at room temperature. About 15 g of sodalite were placed in a thimble and continuously refluxed for 3 days in a Soxhlet extraction apparatus with 500 mL deionized water. Concentrated H_2SO_4 (2 mL) had been added to the water to prevent foaming and improve the extraction efficiency.

Silver Exchange

Melt Exchange

Silver-containing sodalites were prepared by a melt ion exchange of a mixture containing the parent sodium sodalite, $AgNO_3$ (Fisher, 99.8%), and, in some cases, $NaNO_3$ (ACS grade) as diluent. Typically, 1-2 g of sodium sodalite was mixed with silver nitrate (m.p. 212°C) in a porcelain mortar. For complete silver exchange a slight excess of silver nitrate was used, while for partial exchanges stoichiometric amounts were used. The mixture was heated in the dark to 230°C for 24 hours (320°C if $NaNO_3$ was used). The products were filtered in the dark through a 0.8 μm cellulose nitrate filter membrane, washed with *ca.* 2 L of deionized water, and dried in air at ambient temperature. Because of their light sensitivity, the white-to-yellow dry powders were stored in dark sample vials.

Aqueous Exchange

An aqueous ion exchange is possible for even milder exchange temperatures (room temperature up to 100°C). Sodium sodalite was added to an aqueous solution containing stoichiometric amounts of silver nitrate. The mixture was stirred in the dark for 24 hours at room temperature. The product was filtered, washed in the dark and dried in air. Analysis by far-infrared spectroscopy showed that replacement of sodium by silver had proceeded to completion, or nearly so.

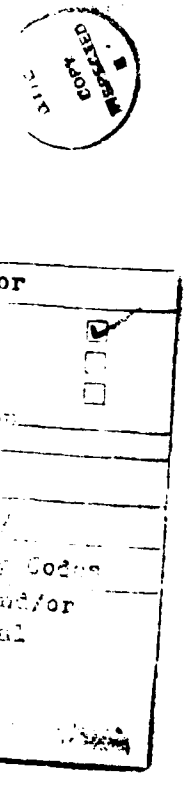

Dehydration

The sodium sodalites were dehydrated under vacuum (10^{-4} - 10^{-6} torr) by the following temperature ramps. Room temperature to 100°C in 30 minutes, held at 100°C for one hour, 100 - 450°C (or 550°C) over 4 hours, and then held isothermally at 450°C (or 550°C) for 1 hour. Since Ag^+ ions are easily reduced, sometimes even after pumping, samples containing Ag^+ were heated to 100°C much more slowly, held at that temperature for a longer time and heated to a lower maximum temperature (*ca.* 300°C - 450°C) than sodium sodalites. Dehydration of relatively open sodalite systems (those containing anion-free cages) occurred at considerably lower temperatures (*ca.* 100°C lower) than for sodalites in which all cages were filled with anions. In the latter, all the <111> channels are blocked by Na^+ ions, and it is only after partial removal of the Na^+ ions from the centers of the 6-membered windows that it becomes possible for the water molecules to leave[5].

The product crystallinity was monitored by powder XRD at each step. The reactions are summarized in the following scheme:

$$Na_8Br_{2-p}(OH)_p\text{-SOD}$$

$$\downarrow \; -pNaOH \text{ (Soxhlet)}$$

$$Na_{8-p}Br_{2-p}[]_p\text{-SOD}$$

$$\downarrow \; +2nAg^+ \text{ (melt)}$$

$$Na_{8-p-2n}Ag_{2n}Br_{2-p}[]_p\text{-SOD} + 2nNa^+$$

Details of the chemical analyses, powder XRD, Rietveld refinement, ^{23}Na MAS and DOR NMR, far-IR, mid-IR, optical reflectance spectroscopy and extended Hückel molecular orbital calculations have been recently described[2].

Product Characterization

Chemical Analysis

Samples containing various substoichiometric amounts of halide have been synthesized with the silver loading varied over the whole range of 2n = 0-8. A chemical analysis (Table

3) showed that the products obtained from the hydrothermal synthesis consisted of both Na_4OH and Na_4Br occupied cages, and that the amount of halide included in the hydroxosodalites was generally much lower than the amount added to the reaction vessel. The isotherm for bromosodalite favors the inclusion of bromide over hydroxide or water[11]. However, as for most sodalites, excess salt is required to form a product in which all cages are filled with monovalent anions. Otherwise, the sodalites contain cages with imbibed hydroxide or water, or completely different phases such as cancrinite can be created[11].

The bromide concentrations were virtually identical for a sodalite before and after Soxhlet extraction. Because of their size ($r(Br^-)$ = 182 pm, C.N. 6)[12] bromide ions were not washed out through the sodalite six-rings (r = 1.10 - 1.30 Å)[13], and their distribution throughout the sodalite lattice could not change after the hydrothermal synthesis.

The sodium aggregates could be progressively exchanged by silver ions to yield at full substitution the corresponding mixture of $(2\text{-}p)Ag_4Br$ and pAg_3 units. A single sodalite phase was observed for a given bulk composition by powder XRD in fully hydrated samples after each reaction step. In a completely silver exchanged sample containing Br^- in 1 out of 8 cages, less than 0.9 mol% Na was found by chemical analysis after aqueous exchange.

Powder XRD - Unit Cell Dimensions

Knowledge of the effect of the sodalite composition on the unit cell size and the interatomic distances is vital to understand the coupling between atoms, and thus the electronic and optical properties of the materials. The unit cell sizes of the Class B sodalites studied are listed in Table 4. The edge lengths of the cubic unit cell depended on the silver and bromide concentrations as well as on the degree of hydration. The response of the sodalite framework to the gradual addition of Br^- anions to the unit cell of Na[]-SOD, eventually yielding NaBr-SOD, is shown for the fully hydrated samples in Figure 1. The interpretation of the unit cell data requires an appreciation of the role of imbibed water. Neutron diffraction studies on Na[]-SOD·nH2O (n = 0, 8)[10,14] demonstrate that the water molecules are both coordinated to the Na^+ six-ring cations and hydrogen-bonded to the framework oxygens. The first Br^- entering the Na_3 cages to form Na_4Br clusters, causes the unit cell to expand (partial loss of structural hydrogen-bonding from β-cage imbibed H_2O) while the further influx of Br^-

up to full loading has a cage contraction effect (electrostatic attraction by Na_4Br formation) as seen by the gradual diminuation of the sodalite unit cell dimension. Upon dehydration the unit cells of these samples expand, thus providing evidence for the retention of some degree of structural hydrogen-bonding in the series of hydrated samples, even in the presence of bromide. A monotonic cage contraction effect with increasing bromide content is observed within the dehydrated series.

In the analogous series of hydrated silver sodalites a slight contraction of the unit cell is observed for higher bromide concentrations (Figure 1). This can again be understood by invoking electrostatic effects due to an interaction between the halide, cations and framework oxygens. The difference in cell dimensions between corresponding sodium and silver sodalites is small, as these cations have nearly identical radii (4-coordinate $r(Na^+)$ = 1.13 Å, $r(Ag^+)$ = 1.14 Å)[12]. The exceptional cell expansions after introduction of silver to bromide-free Na[]-SOD may be related to differences in hydrogen bonding for the two cations, water and framework oxygens. This effect will be discussed later in more detail.

In contrast to the bromo, hydrosodalites, NaBr[]-SOD, the unit cell of the hydrated bromo, hydroxosodalites, NaBrOH-SOD increases monotonically as the bromide content rises. In this case the effect is spatial, the larger bromide ion requiring more room than the hydrated hydroxide ion. In basic sodalite no essential H-bonding exists between framework oxygens and those of the trapped water/hydroxyl groups, and the unit cell is known to contract after dehydration[15,16].

Rietveld Refinement

Class B sodalites can be compared to the mineral nosean[17,18]. Nosean has the ideal composition $Na_8[Al_6Si_6O_{24}]SO_4 \cdot H_2O$ and contains ordered clusters of the types $[Na_4 \cdot SO_4]^{2+}$ and $[Na_4 \cdot H_2O]^{4+}$ in a 1:1 ratio. The ordering has been ascribed to a difference in the net charge and size of these clusters. Antiphase domain boundaries arise from the ordering of clusters. Each domain belongs to the space group P23, a subgroup of $P\bar{4}3n$. The average space group is $P\bar{4}3n$. The cluster ordering leads to positional modulations of the framework oxygens, *i.e.*, two well defined framework oxygen atom positions in nosean. Super-

structure reflections in sulfatic sodalites generally do not give rise to an integral multiple cell[19]; their superstructures are thus incommensurate[17,18].

Rietveld refinements of high resolution powder XRD data were carried out on several samples of the $Na_{8-2n-p}Ag_{2n}Br_{2-p}[]_p$-SOD series for n = 0, p = 0, 1.7, 2 and n = 4, p = 0, 0.8, 1.5, 1.7, 2. The crystallographic data are given as Supplementary Material. No superstructure reflections were observed in the powder patterns, indicating the absence of guest ordering. Only one average type of framework oxygen was therefore refined. Si-Al ordering in the framework was indicated by the ^{29}Si MAS NMR spectrum of typical silver exchanged parent materials which exhibited only one sharp peak (NaAgBrOH-SOD BrLIII, 2Ag/u.c., a_o = 8.929(2) Å, -85.3 ppm *versus* TMS; AgOH-SOD, a_o = 8.786(2) Å, -81.3 ppm; compared to *e.g.*, NaOH-SOD, -84.3 ppm hydrated, -81.0 ppm dehydrated[20]). Most samples refined well assuming an average space group $P\bar{4}3n$ and a solid solution of cages (commensurate) with or without bromide ions, Figure 2. With the exception of one sample, all R-factors were in the ranges wR_p: 9.8 - 13.5 %, R_p = 7.3 - 9.9 %, so that good unit cell sizes as well as the locations and separations between framework and guest atoms could be determined. Table 5 summarizes the results from the refinements and lists structural parameters of related sodalites from the literature.

One may expect silver to occupy more than one type of position, depending on the additional guest species present in each cage. Structural refinements were therefore carried out using one average type of silver (both, isotropic and anisotropic temperature factors), or two types of silver atoms (corresponding to silver tetrahedra and silver triangles with vertices situated on the three-fold axes near the sodalite six-rings), Table 6. The Ag-X distance (X = Br or center of cage) obtained from the isotropic calculations turned out to be the mole-fraction weighted average of the two distances obtained in the calculation where two silver atoms were allowed. The two positions were so close (within 0.26 Å) that they could not be reliably resolved by using a scan range to 100°2θ with Cu-Kα radiation. An EXAFS analysis[21] was also unable to distinguish between two silver sites. Even when anisotropy was invoked, the final temperature factors refined to nearly spherical symmetry. The R-factors for each calculation were so similar that a choice between the three alternatives could not be made. Data corresponding to the average isotropic silver atoms are presented here.

Because of the presence of hydrogen bonding in hydrated samples, the cage dimensions and Al-O-Si angles depend strongly on the water content. For example, in Na[]-SOD, depending on the degree of dehydration, a_o varies from 8.87 (4 H_2O/cage) to 9.11 Å (no H_2O)[5]. Any ions that interact with water have a significant effect on unit cell parameters. The effect of hydrogen bonding leads to a much larger range of Al-O-Si angles than in Class A and Class C sodalites[2,22]: 133 - 156°. The increase in range also applies to the x, y and z coordinates of framework oxygens which are involved in the hydrogen bonding.

In situations where water is not hydrogen bonded (NaOH-SOD) it performs only a space-filling role. Complete dehydration results in a contraction of the cage[10]. However, whenever hydrogen-bonding *via* the water occurs, as in Na[]-SOD, the water pulls the six-ring oxygen atoms closer together (distance of framework oxygens to center of six-ring: Na[]-SOD_{hyd} < NaBr-SOD < NaBr[]-SOD BrLI < < $Na[]\text{-}SOD_{dehyd}$); the concomitant tilting causes a cage contraction. In addition, a strong interaction between sodium ions and water oxygens draws the water molecules towards the sodium ions. The $Na\text{-}O_{water}$ distance of 2.44 - 2.46 Å compared well with the literature distance[23] reported for aqueous sodium ions: 2.40 - 2.50 Å. With tetrahedral arrangements of cations and water (or pseudotetrahedral for three cations in four sites), the net pull is toward the center of the cage, resulting in cage contractions (distance of framework oxygen to center of cage: $Na[]\text{-}SOD_{hyd}$ < NaBr-SOD < NaBr[]-SOD BrLI < < $Na[]\text{-}SOD_{dehyd}$). In those instances, dehydration removes the "ties", yielding a cell expansion[10].

The present study has shown that addition of a little silver to hydrated Class B sodalites causes a large unit cell size increase. This effect cannot be spatial as the ionic radii of four-coordinate Ag^+ and Na^+ are virtually equal. It is proposed that the expansion originates from the different hydration tendencies of Ag^+ compared to Na^+. For low hydration numbers, gas phase silver ions have been shown to bind to water more strongly than sodium ions[24]. This behavior has been related to the tendency of silver ions to exhibit two-fold coordination due to mixing of d_{z2}, s and p_z orbitals[25]. In the confinement of the sodalite cage, however, linear coordination with water is not possible. The refinement data show that silver ions are less strongly associated with the water molecules than the sodium ions are (longer cation-water oxygen separation: > 2.8 Å, compared to literature values[23] of aqueous Ag^+:

2.31 - 2.43 Å). The water molecules are not drawn as closely to the silver ions and therefore move closer to the six-rings. While the six-ring oxgyens are still bridged by water molecules through hydrogen bonding ($d(O_{framework} - O_{water}) < 3.5$ Å in all cases[10]), they are now not pulled strongly to the cation. In this case a less favorable orbital overlap between silver and water may lead to a lower binding energy compared to sodium, resulting in the longer cation-water separations, that were observed in the silver sodalites. As soon as the first silver ion is added, it breaks the tetrahedral symmetry of the cation cluster. The net force on the water molecules which pull the framework oxygens is no longer towards the cage center, although framework distortion may still occur. The result is a drastic framework expansion even at low silver concentrations (see Figure 3).

In the hydroxide series a small addition of silver also causes a drastic expansion of the unit cell. In hydroxosodalites, hydrogen bonding between the framework and guest constituents is not invoked, as the separation between framework oxygens and oxygens in the complex cation $(Na_4OH \cdot H_2O)^{3+}$ exceeds 3.5 Å [10]. Because of the different hydration behavior for Na^+ and Ag^+, replacement of Na^+ by Ag^+ ions may lead to rearrangement of the complex cation and change its space-filling character, resulting in the observed unit cell expansion.

Anion Distribution

Spectra obtained by mid- and far-IR, MAS-NMR, and powder XRD showed single sets of peaks whose positions depended on the sample composition, rather than revealing a superposition of peaks corresponding to the end members of the series ($p = 0, p = 2$). These results point to a 3-D commensurate, compositionally disordered solid-solution model, instead of one involving ordering (crystallographic superlattice), domains or complete segregation of M_4Br and M_3 aggregates ($M = Na^+, Ag^+$). The $(2-p)M_4Br$ clusters are randomly organized in the sodalite lattice of pM_3 spectator cationic triangles.

Cation Distribution

In partially silver exchanged Class A sodalites, where every β-cage is filled with only one type of halide anion, silver is distributed randomly throughout the lattice[2]. However, for Class

B sodalites, both UV-visible reflectance and double rotation (DOR) ^{23}Na-NMR spectroscopy provided evidence for preferential silver aggregation in halide-containing cages over anion-free cages at intermediate bromide and silver loadings. Figure 9 shows UV-visible reflectance spectra for the whole range of bromide concentrations of NaAgBr[]-SOD with 2 and 8 Ag/unit cell, respectively. At full silver exchange, but intermediate Br loading, the spectrum shows features associated with silver in both Br-cages and []-cages (see below). In only partially silver exchanged NaAg[]-SOD, a strong absorption due to Ag^+ in the anion-free cages is observed. However, when bromide is present in partially exchanged samples, absorption features pertaining to silver in bromide cages predominate in all cases, indicating that silver aggregates preferentially in the halide-containing cages, where stronger covalent bonding between Ag-X is possible.

NMR spectroscopy (see below) was utilized to monitor the changes that occurred at specific cation sites after silver exchange. Figure 4a shows ^{23}Na DOR NMR spectra of NaAgBr[]-SOD, BrLIII (Table 3) containing 2 and 1 Ag/unit cell and their silver free parent sodalite. In the parent material, two sodium resonances are observed, at 5.3 ppm *versus* a dilute aqueous NaCl solution (associated with Br-cages) and -4.6 ppm (associated with []-cages). For silver exchanged samples, the intensity of the resonance corresponding to the Br-cages is progressively reduced with increasing silver content. At the same time the second resonance remains at nearly constant intensity. In samples with lower bromide loading (BrLI) the high frequency resonance disappeared almost completely after 2 Na^+ ions per unit cell had been replaced by silver, Figure 4b. The loss in intensity indicates that the sodium concentration is reduced in those cages containing bromide before the ones containing no anion. Similar observations were made in NaAgBrOH-SODs. Extended Hückel molecular orbital calculations have shown that in NaAgX-SOD a bonding MO interaction exists between Ag-orbitals and X-orbitals. On the other hand, in NaAg[]-SOD no overlap of bonding orbitals of Ag with any other species develops (water not considered). Because of the strength of the silver-bromide bond, there is a clear preference for the silver to exchange sodium cations in bromide cages, rather than exchanging sodium in empty or hydroxide cages. Domains of higher silver concentration were too small (50 - 200 Å) to be resolved by powder X-ray diffraction, as they are controlled by the solid solution model proposed for the anions, above.

Cluster Interactions: Vibrational Coupling

A comparison of the trend in atomic separations (Table 5) with the corresponding far-IR spectra reveals a dependence of the vibrational coupling on the bromide content of these samples. The far-IR spectra for samples with varying bromide content (Figure 5a) show the effect of dropping the population of Na_4Br clusters from two to zero per unit cell of sodalite. The smoothness of this transformation is demonstrated by the monotonic low frequency shift of the pore opening framework mode with decreasing halide concentration (Figure 5b). The splitting of the Br^- anion correlation couplet[26] seen at 161 and 68 cm^{-1} decreases as the average separation between bromides becomes greater (larger p) (Figure 5c). Its intensity subsequently goes to zero. However, the Na^+ cation correlation couplet observed at 200 (E) and 105 cm^{-1} (A_1) remains, and each band broadens, due to an inhomogeneous distribution of Na_4Br/Na_3. Even at one Br^- every fourth cavity (p = 1.54), the collective vibrational coupling between Na_4Br clusters has been severely suppressed. The absence of the correlation splitting in Na[]-SOD [26] demonstrates the requirement of Br^- for effective coupling between the Na^+ ions of adjacent β-cages.

The correlation splitting between the sodium translational modes decreases slightly as bromide is added to the sodalite. If the coupling depended solely on the separation between Na^+ ions in adjacent cages one would expect the opposite trend, since the Na-Na separation between adjacent cages was found to decrease at higher Br loadings. However, the Na-X separation increases at the same time. This provides further evidence that the anion plays a significant mediation role in the coupling between Na^+ ions. Since non-basic hydrosodalite, containing only cationic triangles exhibits no correlation coupling, it is likely that at dilute bromide concentrations the Na^+ coupling occurs predominantly between cages containing sodium tetrahedra. The overall effect is therefore complicated by the extent of connectivity between MBr_4 clusters throughout the lattice. Similar, but less pronounced effects can be discerned in the far-IR spectra of the corresponding fully Ag^+ exchanged $Ag_{3-p}Br_{2-p}[]_p$-SOD. The Ag-X distance decreases at higher Br^- loadings. One might expect an increase in Ag-Ag correlation coupling. Unfortunately the correlation couplet A_1 type partner of the E-type

silver translational mode at 91 cm^{-1} was not observed in the experimental range down to 50 cm^{-1}, and the above idea could not be tested with the silver samples.

Cluster Interactions: Electronic Coupling

Solid State NMR

Evidence for collective electronic interactions stems from both the ^{23}Na NMR spectra and UV-visible absorption spectra. ^{23}Na MAS NMR spectra of hydrated Class B sodium sodalites show two components, a sharp band (full width at half height (FWHH): 310 - 380 Hz) *ca.* 1 ppm upfield from solid NaCl and a broad band (FWHH: 1200 - 1350 Hz) *ca.* 17 ppm upfield from the reference sample, Figure 6. The relative intensity of the sharp to the broad absorption increases as more bromide is added. In a sample which contains essentially all Br cages, the band at -17 ppm is virtually absent*. One may therefore assign the broad resonance to sodium in anion-free cages. A linear correlation between the ratios of sodium in Br and [] cages obtained from a chemical analysis and the ratios of the two peak areas confirms the assignment. Rapid chemical exchange between the two cation sites, which has been observed in other hydrated zeolite samples[27], did not occur, as it would have produced a single Na^+ line. Double rotation ^{23}Na MAS NMR spectra[28] show the same two features, indicating that quadrupolar effects can be neglected in the qualitative interpretation of these spectra, Figure 7.

In dehydrated samples only one resonance is observed, which increases in intensity and shifts downfield with higher Br^- loading. This peak is assigned to the ^{23}Na resonance in cages containing Na_4Br. The absence of an observable peak corresponding to Na_3 cationic triangles indicates that intensity loss has occurred through line broadening as a result of greater localization of cations in the cation sites of the []-cages[29], and of locating the bare Na^+ ions in less symmetric environments than hydrated sodium ions[30]. This greatly increases the

* A small remnant is an indicator for some defects: hydroxide or water-containing cages. It may be used as a gauge to estimate the concentration of such defects.

quadrupolar interactions[31] *. Chemical exchange of Na^+ between cages is not expected at room temperature for dehydrated sodalites[27]. In the dehydrated samples the shift of the Na_4Br resonance with increasing Br^- loading is attributed mainly to deshielding of sodium due to electron withdrawal by the relatively electronegative bromide ion, thereby providing evidence for electronic coupling between Na4Br clusters. Any effects involving charge transfer by framework oxygens must be negligible as they would result in the opposite trend: as the bromide concentration increases, the unit cell size and T-O-T angles both decrease[34], allowing more charge density to relocate from the sodalite-cage lattice six-ring oxygen to Na^+(3s), especially as the Na-O separation is reduced at the same time. As in the case of the unit cell sizes, one has to consider the role of imbibed water to interpret the ^{23}Na chemical shifts of the hydrated bromo, hydrosodalites. In these samples, as the Br^- loading increases the water content correspondingly decreases. The structural water in the cages containing cationic triangles has the effect of deshielding the sodium cations in bromide-containing β-cages. This occurs presumably by withdrawing charge density from the framework oxygens *via* hydrogen-bonding.

^{23}Na MAS NMR spectra for samples containing both OH^- and Br^- anions, (*i.e.*, the precursors to the above samples, before Soxhlet extraction) are shown in Figure 8. They are all similar in appearance to spectra for samples without OH^-. Small differences in chemical shift can be related to different unit cell sizes for the two materials, the shift becoming more negative for larger unit cell sizes, Table 7. In these samples some NaOH may have been removed during the washing process, possibly resulting in a mixture of OH and []-cages.

Optical Spectroscopy

Optical reflectance data for $Na_{8-p-2n}Ag_{2n}Br_{2-p}[]_p$-SOD where p = 0-2, 2n = 0-8 are shown for the hydrated samples at room temperature in Figure 9. The series p = 2, 2n = 0-8 serves as a pivotal control group to pinpoint those absorptions associated with m = 0-3

* In a hydrated sample the electric field gradient produced by induced dipoles at the sites of the oxygen ions[32] is averaged by the motion of water molecules[33].

$Na_{3-m}Ag_m$ ionic triangles, which all fall at 220-240 nm and 300 nm (Figure 9A). The absorption in the silver-free Na[]-SOD occurs at lower energy (240 nm) than in NaBr-SOD. Extended Hückel molecular orbital (EHMO) calculations indicate that this is due to the stabilization of the {Si 3s, 3p, Na 3s} levels in Na[]-SOD compared to a sodium halosodalite, Figure 10. The framework O 2p levels fall in the same energy range, whether or not the halide is present.

When silver is introduced into the anion free sodalite, an absorption band due to the {Ag 5s, Na 3s, Si 3s, 3p} ← {Ag 4d} transition and/or the {Ag 5s, Na 3s, Si 3s, 3p} ← {Ag 5p, 4d} transition appears in the UV region. At low silver ion loading the corresponding filled molecular orbitals (MO) are split and structure can be observed in the optical spectrum. At higher concentrations of silver the splitting disappears as the individual MOs appear to form a valence band. At full silver exchange another absorption band is observed at *ca.* 305 nm. This is assigned to the {Ag 5s, 5p} ← {Ag 4d} transition, as the {Ag 5s, 5p} levels have now split away from the {Si 3s, 3p} band. In contrast to the other electronic transitions mentioned here, this transition occurs purely within cluster atoms, and does not involve the framework.

Now let us consider the effects of including increasing loadings of bromide in the sodalite cages. For one Br^- in every eighth sodalite cage, the linewidths of the $Na_{4-n}Ag_nBr$ cluster UV optical excitations are so narrow compared to the parent case of one Br^- per cavity (Figure 5-11B), that individual components for n = 0, 0.05, 0.5 1, 4 can be resolved around 230, 248, 250/265, and 255/270/320 nm, respectively. When these data are compared with those of Class A quantum supralattices[1,2] (Figures 9Ce, De, Ee), one realizes that all of the resolved components of the Class B supralattice are contained within the spectral envelope of the former. The absorption bands can be assigned by assuming a superposition of contributions from M_3^{3+} and M_4X^{3+} containing cages. For example, in the sodalite containing isolated Ag_4Br^{3+} clusters (Figure 9Be or Fb) the absorptions at *ca.* 230 and 320 nm can be assigned to the {Si 3s, 3p} ← {Ag 4d} and {Ag 5s, 5p} ← {Ag 4d} transitions, respectively, for Ag_3^{3+} cages; and those at *ca.* 255 and 270 nm to the {Ag 5s, Si 3s, 3p} ← {Ag 4d} and {Ag 5s, Si 3s, 3p} ← {Br 4p, Ag 5s, 5p, 4d} transitions, respectively, for Ag_4Br^{3+} cages. These assignments are consistent with all spectra shown in Figure 9, as well as in the iodide equivalents (replacing Br 4p by I 5p) shown in Figure 11.

At low silver and bromide loadings the very sharp UV absorption spectrum resembles that of an isolated gas phase silver bromide monomer ({Ag 5s} ← {Br 4p, Ag 4d}), Figure 9Bb. It is notable that the Ag-Br bond length in NaAgBr[]-SOD BrLI, 1Ag/u.c. (corresponding to spectrum 9Bc) has the same value as that of a gas phase AgBr molecule (2.39 Å[35], and is much shorter than the Ag-Br distances in completely silver exchanged samples[2].

The reader should note that one cannot truly speak of an "isolated molecule". The observed electronic transitions do not occur completely within the molecule, but also involve the lattice. Orbital overlap of the silver cation 5s and 5p orbitals with the halide anion, sodium cations as well as framework atoms is significant (*ca.* 8 - 28%). A more accurate term would be "a defect AgBr molecule in the Na[]-SOD lattice". In fact, one cannot even speak of Ag_4Br^{3+} as an "isolated cluster". Here, too, the framework is involved in the electronic transitions, and significant overlap exists between the Ag^+ and framework constituents. Host matrix effects must therefore be considered.

The line broadening and red shift of the bandedge observed when either the silver or the bromide concentration is increased indicates electronic coupling between $Na_{4-n}Ag_nBr$ clusters (Figure 9F). The absorption edge extends even further into the red for bulk AgBr[2]. Whereas sodium does not appear to contribute much to the coupling (the absorption bands are sharpest at high sodium concentrations), both bromide and silver must be mediating the communication between clusters. The Ag-Br and Ag-Ag separations (within each cage) change most drastically between p = 1.7 and p = 1.5. However, the most significant broadening of absorption bands in the optical spectra occurs only after the p = 0.8 loading level. This is an indication that the major mechanism leading to band broadening is not an increase in orbital overlap of the ions within a cage, but rather greater communication between clusters in adjacent cages, as the number of bromide centers rises and their separation decreases. Broadening due to phonon coupling is an additional factor. For example, upon cooling AgBr-SOD to 27K three major components could be ~~resolved~~ completely and ~~further~~ other-mem components partially resolved.

EHMO Calculations - Development of Bands

The density of states diagrams for one and ten Ag_4Cl clusters (in which the sodalite framework was not included) show the origin of band broadening as clusters couple (Figure 12). Even at the low aggregation number of ten clusters, the density of states increases. By extrapolation, continuous band formation becomes possible at approximately Avogadro's number of clusters. Nevertheless, a simple increase in the density of states does not imply band formation. For that to happen, the orbitals must overlap significantly. Overlap values are proportional to the interaction between atoms[36]. An EHMO calculation[37] revealed that at a separation of 4 - 5 Å between silver atoms within a cluster and between clusters, the overlap is up to 19 and 13 %, respectively. Because of the large separation between clusters, the bands formed by the quantum supralattice are expected to be narrow. However, k-space band calculations would be required to probe the bandwidth.

The effect of the number of clusters, n, on the frontier orbital levels was studied for $[Ag_3^{+3}]_n$ clusters, arranged in a space-filling cubic arrangement, as they would be in a cube of nine sodalite cages, Figure 13. Even though the absolute energies obtained with and without charge iterations differed greatly, the general trend observed was the same. For aggregations of $[Ag_3^{+3}]_n$ clusters the HOMO-LUMO gap remained nearly constant as n increased. This is in contrast to $[Ag_4Cl^{+3}]_n$ clusters, for which the gap was reduced for larger n [2].

Class B sodalites contain mixtures of cages with different guest clusters. Figure 14 shows the trend in frontier orbital energies going from $[Ag_4Cl]_9$ to $[Ag_4Cl]_8[Ag_3]$, $[Ag_4Cl][Ag_3]_8$ and finally $[Ag_3]_9$ cluster aggregates. By coincidence, the energy gap in the end members is similar (374 nm and 395 nm for $[Ag_4Cl]_9$ and $[Ag_3]_9$, respectively). The LUMO's are composed of Ag 5s (some Ag 5p) and the HOMO's of Cl 3p, Ag 4d, Ag 5s or only Ag 4d of their respective clusters. It is noteworthy that as soon as one different cluster is added as an "impurity" the gap becomes narrower and remains nearly unchanged with the relative ratio of the two types of clusters. The main reason for the constant gap is the fact that the HOMO level always is associated with an Ag_4Cl^{+3} cluster and the LUMO with an Ag_3^{+3} cluster. Both of these orbital levels are only weakly dependent on the cluster size. The frontier levels of these clusters are only slightly perturbed by their neighbors. Atomic charge calculations showed that the

silver atoms in Ag_3^{+3} clusters retain their full charge (+1) while in Ag_4Cl^{+3} clusters the charge is alleviated by the Cl-atoms (+0.46). This implies that the two types of cluster do not form mixed bands (one would otherwise expect some alteration of the charge on Ag_3^{+3} clusters) and that at low "defect" concentrations the "defect" clusters may indeed be considered isolated. Based on similar types of calculations for the Class A sodalites[2], we do not expect the inclusion of the sodalite framework to significantly affect the trends and conclusions presented above.

Conclusions

By varying the silver and halide loading of Class B sodalites it is possible to create β-cage encapsulated guests covering the range from an isolated Ag-X molecule to an isolated Ag_4X^{3+} cluster and an extended $(Ag_4X^{3+})_n$ cluster lattice ("expanded semiconductor"). The term "isolated" in this context means isolated from other species of the same type. The justification for using the term Ag-X molecule lies in the fact that the halide appears to be more closely associated with the silver ion than the sodium cations (bond lengths). In case of the isolated molecule and cluster, the electronic states are localized. Formation of an extended cluster lattice leads to cluster interaction *via* vibrational and electronic coupling and possibly to delocalization. The concentration and identity of cations and anions control the extent of coupling, as shown by far-IR, ^{23}Na MAS NMR and UV-visible spectroscopy. Results from optical spectroscopy and extended Hückel molecular orbital calculations hinted at the evolution of narrow bands.

Acknowledgments

We wish to acknowledge the Natural Science and Engineering Research Council (N.S.E.R.C.) of Canada's Operating and Strategic Grants Programmes, Alcan Canada and Optical Recording Corporation, Toronto (G.A.O.), as well as the Office of Naval Research (G.D.S.) for generous financial support of this work. A.S. would like to thank N.S.E.R.C. for a 1967 Science and Engineering Postgraduate Scholarship. We wish to thank Raz Jelinek, Peter M. Macdonald, Michele Meszaros, Bill Harrison and Nancy Keder for valuable technical assistance and discussions.

Table 1. Gel compositions for sodalite syntheses.

Product	$xAl(OH)_3$	$ySiO_2$	$zNaOH$	vH_2O	wNaX	Salt
NaOH-SOD BrL0	1	1	5	41	0	-
NaBrOH-SOD BrLI	1	1	5	41	0.070	NaBr
NaBrOH-SOD BrLII	1	1	5	41	0.0135	NaBr
NaBrOH-SOD BrLIII	1	1	5	41	0.20	NaBr
NaBrOH-SOD BrLA	1	1	5	41	0.625	NaBr
NaBrOH-SOD BrLB	1	1	5	41	0.94	NaBr
NaBr-SOD BrLF	1	2	8	100	5	NaBr
NaIOH-SOD ILI	1	1	5	41	0.070	NaI

Note: All values are given in moles, relative to 1 mole $Al(OH)_3$.

Table 2. List of reagents for sodalite synthesis and silver exchange.

$Al(OH)_3$:	Fisher, 99.8%
SiO_2:	Ludox HS-30, Ludox HS-40 (Dupont), Luddy (40%, Alchem) (colloidal aqueous silica sources)
NaOH:	Mallinckrodt, 98.7%
H_2O:	deionized
NaBr:	Mallinckrodt, 99.0%
NaI:	BDH, 99.0%
$AgNO_3$:	Fisher, 99.8%
$NaNO_3$:	Fisher, certified ACS grade

Table 3. Compositions of Class B Sodalites.

Chemical Analysis

Sample	%Na	%Ag	%Br	%Si	%Al	%O*	ppmFe	Si/Al
Na[]-SOD BrL0	14.73	0.00	0.00	20.25	18.98	46.02	160	1.02
NaBr[]-SOD BrLI	14.39	0.00	2.39	19.68	18.42	45.11	130	1.03
NaBr[]-SOD BrLII	14.76	0.00	4.28	19.99	18.60	42.36	110	1.03
NaBrOH-SOD BrLI	16.68	.0.00	2.45	18.74	17.87	44.24	160	1.01
AgBr[]-SOD BrLI	0.115	40.84	1.86	11.06	10.87	35.26	4420	0.98
NaBr-SOD BrLF	16.27	0.00	13.70	16.17	15.03	38.83	47	1.03

Sample	Composition	Total M^+/u.c.
Na[]-SOD BrL0	$Na_{5.40}Si_{6.07}Al_{5.93}O_{24.2}$	5.40
NaBr[]-SOD BrLI	$Na_{4.49}Na_{1.04}Br_{0.26}Si_{6.08}Al_{5.92}O_{24.4}$	5.44
NaBr[]-SOD BrLII	$Na_{3.66}Na_{1.84}Br_{0.46}Si_{6.10}Al_{5.90}O_{22.7}$	5.50
NaBrOH-SOD BrLI	$Na_{5.17}OH?Na_{1.11}Br_{0.28}Si_{6.02}Al_{5.98}O_{25.0}$	6.55
AgBr[]-SOD BrLI	$Ag_{4.3}Ag_{1.4}Br_{0.35}Si_{5.93}Al_{6.07}O_{33.2}$	5.70
NaBr-SOD BrLF	$Na_{7.50}Br_{1.82}Si_{6.10}Al_{5.90}O_{25.7}$	7.50

Samples were dehydrated under vacuum at 500°C for 1 hour.

Neutron Activation Results

Sample	Composition	Tot. Na/u.c.	Feed Br/u.c.
Na[]-SOD BrL0	$Na_{5.73}$-SOD	5.73	0.00
NaBr[]-SOD BrLI	$Na_{4.64}Na_{1.16}Br_{0.29}$-SOD	5.80	0.42
NaBr[]-SOD BrLII	$Na_{3.95}Na_{2.1}Br_{0.53}$-SOD	6.05	0.81
NaBr[]-SOD BrLIII	$Na_{1.94}Na_{4.72}Br_{1.18}$-SOD	6.66	1.2
NaBr[]-SOD BrLA	$Na_{1.17}Na_{5.56}Br_{1.39}$-SOD	6.73	3.8
NaBr[]-SOD BrLB	$Na_{0.94}Na_{6.52}Br_{1.63}$-SOD	7.46	5.6
NaBr-SOD BrLF	$Na_{7.36}Br_{1.63}$-SOD	7.36	7.5
NaOH-SOD BrL0	$Na_{6.57}OH_?$-SOD	6.57	0.00
NaBrOH-SOD BrLI	$Na_{5.57}OH_?Na_{1.16}Br_{0.29}$-SOD	6.73	0.42
NaBrOH-SOD BrLII	$Na_{4.66}OH_?Na_{2.04}Br_{0.51}$-SOD	6.70	0.81
NaBrOH-SOD BrLIII	$Na_{2.22}OH_?Na_{5.16}Br_{1.29}$-SOD	7.38	1.2
NaBrOH-SOD BrLA	$Na_{1.93}OH_?Na_{5.76}Br_{1.44}$-SOD	7.69	3.8

Samples were hydrated. Feed Br/u.c. is the expected bromide concentration from the feed composition, assuming all bromide present in the reagents enters the product.

Sample	Water of Hydration (non-surface)
NaBr[]-SOD BrLI	5.9 %
AgBr[]-SOD BrLI	4.7 %

Table 4. Unit cell sizes (Å) of Class B sodalites.

NaAgBr[]-SOD

Br Loading	Ag Loading (Ag/u.c.)					Dehydrated
(Br/u.c.)	0	0.1	1	2	8	0
0.00	8.854(3)	8.963(2)[a]	8.959(2)	8.969(2)	8.975(4)	9.092(2)
0.26	8.972(3)	8.965(1)	8.957(3)	8.954(2)	8.966(2)	9.053(3)
0.46	8.964(4)	8.964(2)	8.956(3)	8.955(2)	8.955(3)	9.019(2)
1.18	8.948(1)	8.946(1)	8.943(1)	8.936(2)	8.938(2)	8.959(1)
1.82	8.927(3)		8.924(3)		8.906(2)	8.958(4)

NaAgBrOH-SOD

BR Loading	Ag Loading (Ag/u.c.)					Dehydrated
(Br/u.c.)	0	0.1	1	2	8	0
0.00	8.902(3)	8.964(2)[b]	8.959(2)		8.949(3)	8.7342(8)[d]
0.29	8.916(3)					
0.53	8.920(3)					
1.18	8.933(2)	8.943(2)	8.936(2)	8.929(2)	8.931(3)	
1.82	8.927(3)		8.924(3)		8.906(2)	

NaAgI[]-SOD ILI

Ag Loading (Ag/u.c.)					
0	0.1	1	2	4	8
8.906(3)	8.967(2)[c]	8.963(2)	8.971(2)	8.978(1)	8.993(2)

Notes: All samples were hydrated, except where indicated otherwise.

a) Second phase: 8.849(3) Å

b) Second phase: 8.852(4) Å

c) Second phase: 8.852(2) Å

Two phases were present in these three samples, probably because at such a low silver loading (0.1 Ag/u.c.) the silver did not penetrate into the centres of the microcrystals, so that a cherry-type system was formed with a higher loading of silver in the outer shell than in the core.

d) Value for dehydrated NaOH-SOD taken from Luger et al.[16]. Dehydrated AgOH-SOD has a unit cell size of 8.786(2) Å.

Table 5. Structural parameters of Class B sodalites.

Sample	Reference	UC Edge (Å)	∠Al-O-Si (°)	C-X (Å)	X-X (Å)	M-M_X (Å)	M-M_i (Å)	M-O (Å)
NaOH-SOD·2H_2O	HASS1983	8.890	138.7	2.70	7.70	4.82	4.41	2.38
NaOH-SOD (dehyd.)	LUGE1987	8.7342	132.9	2.40	7.56	4.92	3.92	2.35
Na[]-SOD·8D_2O	FELS1987	8.8160	-	-	-	5.05	3.77	2.47
Na[]-SOD·8H_2O	FELS1986	8.848	136.2	-	-	5.08	3.76	2.51
Na[]-SOD (dehyd.)	FELS1986	9.122	156.3	-	-	4.58	6.06	2.56
NaBr[]-SOD BrLI	own	8.9615	142.0	2.76	7.76	4.84	4.51	2.45
NaBr-SOD	own	8.9305	140.6	2.89	7.73	4.74	4.72	2.36
Na_7Ag_1Br[]-SOD BrLI	own Na	8.9581	141.1	2.83	7.76	4.79	4.62	2.40
	Ag			2.39		5.01	3.89	2.62
Ag[]-SOD	own*	8.9803	-	-	-	4.85	4.53	-
AgBr[]-SOD BrLI	own	8.9566	142.8	2.80	7.76	4.81	4.57	2.41
AgBr[]-SOD BrLII	own	8.9542	143.7	2.68	7.75	4.88	4.38	2.49
AgBr[]-SOD BrLIII	own	8.9306	137.9	2.68	7.73	4.87	4.38	2.38
AgBr-SOD	own	8.9109	141.7	2.67	7.72	4.86	4.36	2.44
Ag[]I-SOD ILI	own*	8.9677	-	2.73	7.77	4.86	4.46	-

Sample	Coordinates Ox	Oy	Oz	M	Water Ox=Oy=Oz	C-OH_2 (Å)	O_1-O_2 (Å)	O-6 (Å)
NaOH-SOD·2H_2O	0.1506	0.4399	0.1397	0.1755	-	-	-	-
NaOH-SOD (dehyd.)	0.1458	0.4265	0.1370	0.1587	-	-	-	-
Na[]-SOD·8D_2O	0.1455	0.4313	0.1363	0.151	0.3773	2.44	2.99	1.94
Na[]-SOD·8H_2O	0.1490	0.4338	0.1366	0.1504	0.3753	2.46	2.96	1.92
Na[]-SOD (dehyd.)	0.1550	0.489	0.1450	0.235	-	-	-	-
NaBr[]-SOD BrLI	0.1504	0.4470	0.1417	0.1779	0.3882	2.73	3.11	2.15
NaBr-SOD	0.1505	0.4439	0.1409	0.1867	-	-	-	-
Na_7Ag_1Br[]-SOD BrLI	0.1506	0.4455	0.1420	0.1825Na 0.1537Ag	0.3938	2.76	3.17	2.23
Ag[]-SOD	-	-	-	0.1782	0.3426	3.03	-	1.44
AgBr[]-SOD BrLI	0.1386	0.4424	0.1323	0.1805	0.3455	3.02	2.80	1.48
AgBr[]-SOD BrLII	0.1443	0.4476	0.1410	0.1730	0.3096	3.26	2.45	0.92
AgBr[]-SOD BrLIII	0.1457	0.4363	0.1379	0.1738	0.358	2.85	2.82	1.67
AgBr-SOD	0.1456	0.4438	0.1393	0.1730	-	-	-	-
Ag[]I-SOD ILI	-	-	-	0.1758	0.3367	3.04	-	1.35

Sample	wR_p	R_p	χ^2
NaBr[]-SOD BrLI	10.6	7.8	3.4
NaBr-SOD	17.0	11.3	6.9
Na_7Ag_1Br[]-SOD BrLI	10.5	7.3	2.9
Ag[]-SOD	13.9	10.6	4.1
AgBr[]-SOD BrLI	10.2	7.7	2.2
AgBr[]-SOD BrLII	9.8	7.3	2.1
AgBr[]-SOD BrLIII	11.4	7.9	3.0
AgBr-SOD	13.5	9.9	2.9
Ag[]I-SOD ILI	13.8	10.7	4.1

See notes on next page.

Table 6. The effect of cation parameters on the refinement of Class B sodalites.

Sample	Refinement	wR_p	R_p	χ^2	M	M-O (Å)	M-X (Å)	M-OH_2 (Å)
NaBr[]-SOD BrLI	Na iso.	10.6	7.8	3.4	0.1779	2.445	2.762	2.73
	Na aniso.	10.4	7.7	3.3	0.1770	2.455	2.748	2.71
AgBr[]-SOD BrLI	Ag iso.	10.2	7.7	2.2	0.1805	2.414	2.800	2.55
	Ag aniso.	10.1	7.5	2.2	0.1800	2.413	2.793	2.55
	2 Ag's iso.	10.1	7.6	2.2	0.188	2.375	2.91	2.44
					0.171	2.472	2.65	2.70
AgBr[]-SOD BrLII	Ag iso.	9.8	7.3	2.1	0.1730	2.487	2.679	2.10
	Ag aniso.	9.6	7.1	2.0	0.1720	2.493	2.668	2.13
AgBr[]-SOd BrLIII	Ag iso.	11.4	7.9	3.0	0.1738	2.379	2.689	
	Ag aniso.	11.3	7.6	2.9	0.1736	2.380	2.686	

Notes for Table 6:
iso. = thermal parameters refined isotropically
aniso. = thermal parameters refined anisotropically

Notes for Table 5: Standard deviations for bond lengths are smaller than the least significant digit shown. All samples were hydrated, except where indicated otherwise. BrLI: 0.26 Br/u.c.; BrLII: 0.46 Br/u.c.; BrLIII: 1.2 Br/u.c. C-X are cation to cage center distances, X-X the anion-anion separations between cages, M-M_X intercage cation separations, M-M_I intracage cation separations, M-O are cation to framework oxygen distances, C-OH_2 the cation-to-water-oxygen distances, O_1-O_2 distances between water oxygens and framework oxygens, O-6 distances between water oxygens and the center of the six-rings. *) Data tentative for this sample due to poor refinement for the framework atoms.

Table 7. ^{23}Na resonances of Class B sodium sodalites.

Sample	Br/u.c.	Treatment	UC Size (Å)	MAS shift (ppm)	R(pk)	R(an)
Na[]-SOD BrL0	0.00	hydrated	8.849	-12.8		
Na[]-SOD BrL0	0.00	hydrated	8.854	-12.6	0.00	0.00
NaBr[]-SOD BrLI	0.26	hydrated	8.972	-1.5, -17.6	0.53	0.24
NaBr[]-SOD BrLII	0.46	hydrated	8.964	-0.9, -17.1	1.42	0.52
NaBr[]-SOD BrLIII	1.18	hydrated	8.948	-1.0, -16.1	6.00	2.43
NaBr[]-SOD BrLA	1.39	hydrated	8.946	-1.2, -17.1	13.3	4.75
NaBr[]-SOD BrLB	1.63	hydrated	8.899	-1.4	15.6	6.94
NaBr-SOD BrLF	1.82	hydrated	8.927	-0.8, -17.5	15.6	7.76

Sample	Br/u.c.	Treatment	UC Size (Å)	MAS shift (ppm)
Na[]-SOD BrL0	0.00	dehydrated	9.092	-15.9
NaBr[]-SOD BrLI	0.26	dehydrated	9.053	-13.9
NaBr[]-SOD BrLII	0.46	dehydrated	9.019	-9.9
NaBr[]-SOD BrLIII	1.18	dehydrated	8.959	-2.9
NaBr-SOD BrLF	1.82	dehydrated	8.958	-0.8

Sample	Br/u.c.	Treatment	UC Size (Å)	MAS shift (ppm)	R(pk)	R(an)
NaOH-SOD BrL0	0.00	hydrated	8.902	-13.8 (-14.0)	0.00	0.00
NaBrOH-SOD BrLI	0.29	hydrated	8.916	-0.8, -16.6	1.08	0.21
NaBrOH-SOD BrLII	0.51	hydrated	8.920	-0.8, -16.4	1.82	0.44
NaBrOH-SOD BrLIII	1.29	hydrated	8.933	-0.9, -15.8		2.32
NaBrOH-SOD BrLA	1.44	hydrated	8.934	-1.0, -17.2	14.8	2.98
NaBr-SOD BrLF	1.82	hydrated	8.927	-0.8, -17.5	15.6	7.76

Notes: MAS shifts are given in ppm versus solid NaCl.

R(pk) refers to the intensity ratios of the high frequency to the low frequency peak. R(an) refers to the analytically determined ratio of Na^+ in Br cages to Na^+ in [] or OH cages (see Table 2-5, Chapter 2). A plot of R(an) versus R(pk) of the first five NaBr[]-SOD samples results in a straight line with a correlation coefficient of 0.998. For the NaBrOH-SOD samples the correlation coefficient is only 0.9996 for all values excluding the last sample which has a great uncertainty in the area of the low frequency peak.

The peak positions of the resonances for the dehydrated NaBrOH-SOD samples were not measured because of strong peak broadening and asymmetry.

References

1. Stein, A.; Ozin, G. A.; Stucky, G. D. *J. Am. Chem. Soc.* 1990, *112*, 904-905.
2. Stein, A.; Ozin, G. A.; Macdonald, P. M.; Stucky, G. D.; Jelinek, R.; Pines, A. *J. Am. Chem. Soc.*, submitted.
3. Stein, A.; Macdonald, P. M.; Stucky, G. D.; *J. Phys. Chem.* 1990, *94*, 6943-6948.
4. Stein, A.; Meszaros, M.; Macdonald, P. M.; Ozin, G. A.; Stucky, G. D. *Adv. Mat.*, in press.
5. Denks, V. P. *Trudy Instituta Fizika Akad. Nauk Estonskoi SSR*, 1984, *55*, 14-71.
6. Stein, A.; Ozin, G. A.; Stucky, G. D. *J. Soc. Photogr. Sci. Technol. Japan* 1990, *53*, 322-328.
7. Hund, F.; Geismar, G. *Chem.-Ztg.* 1990, *114*, 243-244.
8. Hassan, I.; Grundy, H. D. *Acta Cryst.* 1983, *C39*, 3-5.
9. Ernst, H.; Pfeifer, H.; Zhdanov, S. P. *Zeolites* 1983, *3*, 209-213.
10. Felsche, J.; Luger, S. *Ber. Bunsenges. Phys. Chem.* 1986, *90*, 731.
11. Barrer, R. M. *Hydrothermal Chemistry of Zeolites*, Academic Press: London, 1982.
12. Shannon, R. D. *Acta Crystallogr.* 1976, *A32*, 751-767.
13. Breck, D. W. *Zeolite Molecular Sieves*, R. E. Kieger Publishing Company: Malabar, 1984.
14. Felsche, J.; Luger, S.; Baerlocher, C. *Zeolites* 1986, *6*, 367-372.
15. Felsche, J.; Luger, S.; Fischer, P. *Acta Cryst.* 1987, *C43*, 809-811.
16. Luger, S.; Felsche, J.; Fischer, P. *Acta Cryst.* 1987, *C43*, 1-3.
17. Hassan, I.; Grundy, H. D. *Can. Mineral.* 1989, *27*, 165-172.
18. Hassan, I.; Buseck, P. R. *Am. Mineral.* 1989, *74*, 394-410.
19. Taylor, D. *Contrib. Mineral. Petrol.* 1967, *16*, 172-188.

20. Engelhardt, G.; Luger, S.; Buhl, J. C.; Felsche, J. *Zeolites* 1989, *9*, 182-186.

21. Moller, K.; Ozin, G. A.; Stein, A., unpublished results.

22. Stein, A. *Ph.D. Thesis* 1991, University of Toronto, Canada.

23. Burgess, J. *Ions in Solution*, Ellis Horwood Ltd.: Chichester, 1988.

24. Peterson, K. I.; Holland, P. M.; Keesee, R. G.; Lee, N.; Mark, T. D.; Castleman, Jr., A. W. *Surf. Sci.* 1981, *106*, 136-145.

25. Cotton, F. A.; Wilkinson, G. *Advanced Inorganic Chemistry*, 4th ed., Wiley, N. Y., 1980, p. 255, p. 263.

26. Godber, J.; Ozin, G. A. *J. Phys. Chem.* 1988, *92*, 2841-2849, 4980-4987.

27. Kundla, E.; Samoson, A.; Lippmaa, E. *Chem. Phys. Lett.* 1981, *83*, 229-232.

28. Jelinek, R.; Chmelka, B.; Pines, A.; Stein, A.; Ozin, G. A., unpublished results.

29. Welsh, L. B.; Lambert, S. L. in Bradley, S. A.; Gattuso, M. J.; Bertolacini, R. J. (eds.) *Characterization and Catalyst Development* 1989, A.C.S. Symposium Series *411*; American Chemical Society: Washington, D.C., 262-272.

30. Engelhardt, G.; Michel, D. *High Resolution Solid-State NMR of Silicates and Zeolites*, John Wiley & Sons, 1987.

31. Tijink, G. A. H.; Janssen, R.; Veeman, W. S. *J. Am. Chem. Soc.* 1987, *109*, 7301-7304.

32. Lechert, H. in Meier, W. M.; Uytterhoeven, J. B. (eds.), *Molecular Sieves*, A.C.S. Advances in Chemistry Series 121; American Chemical Society: Washington, D.C.; 1974, 74-86.

33. Klinowski, *J. Prog. Nucl. Magn. Reson. Spectrosc.* 1984, *16*, 237-309.

34. Weller, M. T.; Wong, G. *J. Chem. Soc., Chem. Commun.* 1988, 1103-1104.

35. Krisher, L. C.; Norris, W. G. *J. Chem. Phys.* 1966, *44*, 974-976.

36. Calzaferri, G.; Forss, L. *Helv. Chim. Acta* 1987, *70*, 465-479.

37. Calzaferri, G.; Forss, L.; Hugentobler, T.; Kamber, I. *ICONC* and *INPUTC*, Fortran software for extended Hückel molecular orbital calculations, Institute for Inorganic and Physical Chemistry, University of Berne, Freiestrasse 3, CH-3009 Bern, 1989.

Figure Captions

Figure 1. Unit cell size *versus* composition diagram for the series of hydrated sodalites of the type $Na_{8-p-2n}Ag_{2n}Br_{2-p}[]_p$-SOD, where p = 0-2, 2n = 0-8.

Figure 2. Sodalite cages showing the positions of anions (•), cations (O) and water molecules.

Figure 3. Proposed hydrogen-bonding effects in NaAg[]-SOD. A) When four Na^+ cations are present the interaction between an O_{water} atom and adjacent cations is equal in all three directions, leading to a net-force on this oxygen towards the center of the cage. The cage contracts (small unit cell). B) When one Na^+ cation has been replaced by Ag^+, the interaction between an O_{water} atom and adjacent cations is not equal in all three directions. The force vectors do not point towards a common intersection. In spite of possible distortions, the net pull is not towards the center of the cage. The unit cell is therefore larger.

Figure 4. ^{23}Na DOR NMR spectra of A) NaAgBr[]-SOD, BrLIII; a) 2 Ag/u.c., b) 1 Ag/u.c., c) 0 Ag/u.c. B)NaAgBr[]-SOD, BrLI; a) 0 Ag/u.c., b) 2 Ag/u.c.

Figure 5. a) Far-IR spectra for the series of dehydrated sodalites of the type $Na_{8-p}Br_{2-p}[]_p$-SOD. i) p = 2, ii) p = 1.7, iii) p = 1.5, iv) p = 0.8, v) p = 0. b) Shift in the far-IR pore opening mode with Br^- loading. c) Changes in the far-IR correlation splitting between the high-frequency and low-frequency modes of Na^+ (Δ) and Br^- (•) with Br^- loading.

Figure 6. a) ^{23}Na MAS NMR spectra of hydrated $Na_{8-p}Br_{2-p}[]_p$-SOD. i) p = 2, ii) p = 1.7, iii) p = 1.5, iv) p = 0.8, v) p = 0. b) The dependence of the ^{23}Na MAS NMR shifts of the Na_4Br resonance relative to solid NaCl on the Br^- concentration for hydrated (•) and dehydrated (O) samples.

Figure 7. ^{23}Na NMR spectra of NaBr[]-SOD, BrLI, showing the similarity between MAS and DOR results for this type of sample.

Figure 8. ^{23}Na MAS NMR spectra of hydrated $Na_8Br_{2-p}OH_p$-SOD. i) p = 2, ii) p = 1.7, iii) p = 1.5, iv) p = 0.8, v) p = 0. Note the similarity with the spectra of the Soxhlet-extracted products of these samples, shown in Figure 6.

Figure 9. Optical reflectance data for some members of the hydrated sodalite series $Na_{8-2n-p}Ag_{2n}Br_{2-p}[]_p$-SOD. A) p = 2, B) p = 1.7, a) n = 0, b) n = 0.05, c) n = 0.5, d) n = 1, e) n = 4. C) n = 0.5, D) n = 1, E) n = 4, a) p = 2, b) p = 1.7, c) p = 1.5, d) p = 0.8, e) p = 0. F) Progression of the UV-visible spectra from the sodalite encapsulated isolated AgBr molecule to the isolated Ag_4Br cluster and to the extended $(Ag_4Br)_n$ quantum supralattice.

Figure 10. Sodalite band diagrams for one cluster of the type indicated, inside a single sodalite cage.

Figure 11. Optical reflectance data of hydrated sodalites of the type NaAgI[]-SOD IL1, with various silver loadings. a) 0 Ag/u.c., b) 1 Ag/u.c., c) 2 Ag/u.c., d) 4 Ag/u.c., e) 8 Ag/u.c.

Figure 12. Density-of-states diagrams for a) Ag_4Cl^{3+} and b) $[Ag_4Cl^{3+}]_{10}$. The graphs show the number of molecular orbitals per atom within 0.25 eV ranges.

Figure 13. The effect of $[Ag_3^{3+}]_n$ cluster aggregation on the frontier orbital energies. +: LUMO (no charge iterations (CI)), []: HOMO (no CI), Δ: LUMO (CI), ◇: HOMO (CI).

Figure 14. The effect of the Cl:[] ratio of Ag_4Cl^{3+} and Ag_3^{3+} cluster aggregates on the frontier orbital energies. Nine clusters were organized in a body centered cubic arrangement for these EHMO calculations.

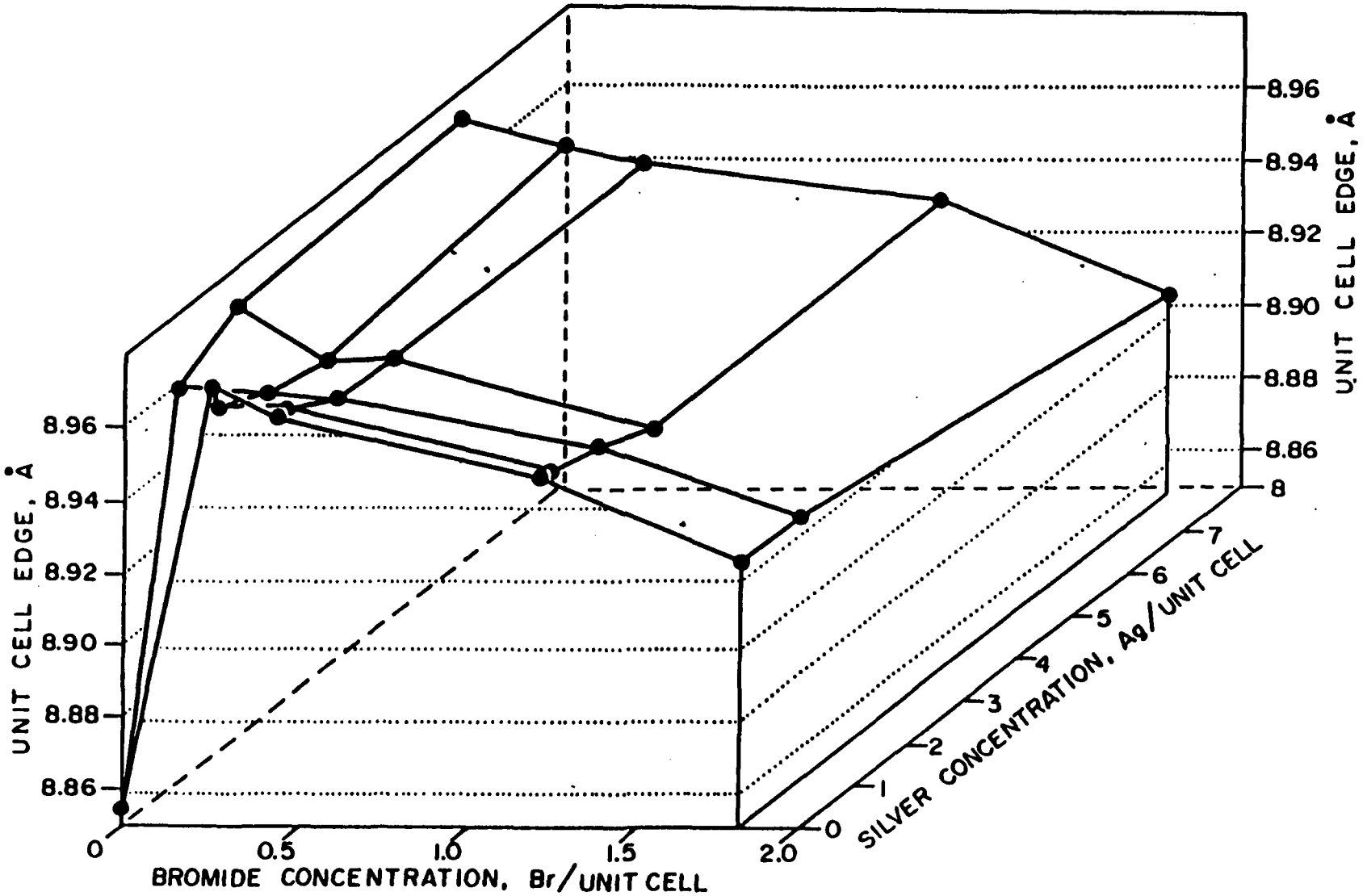
UNIT CELL EDGE, Å
8.96
8.94
8.92
8.90
8.88
8.86
0
0.5
1.0
1.5
2.0
BROMIDE CONCENTRATION, Br/UNIT CELL
SILVER CONCENTRATION, Ag/UNIT CELL
0
1
2
3
4
5
6
7
8
8.86
8.88
8.90
8.92
8.94
8.96
UNIT CELL EDGE, Å

F1

F2

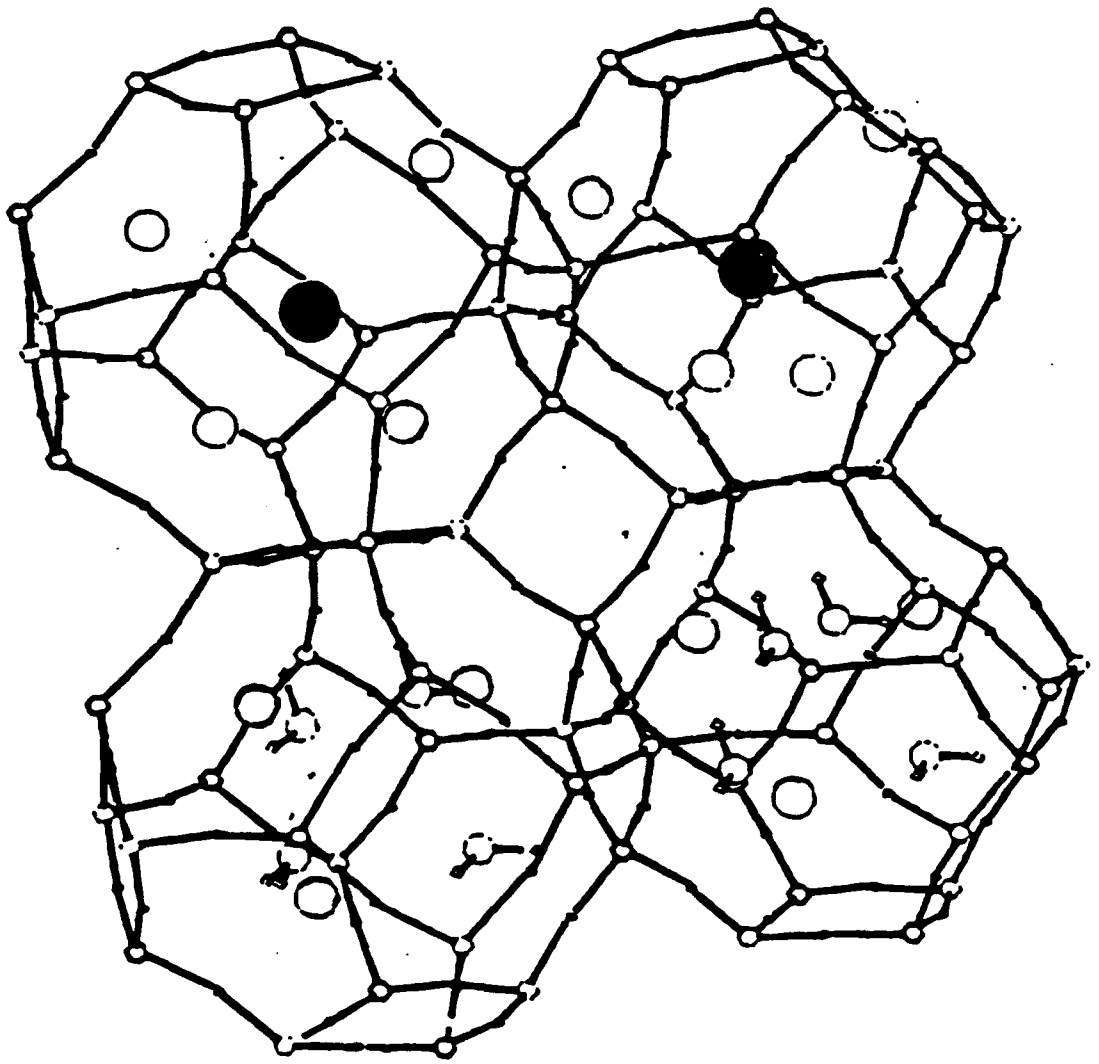

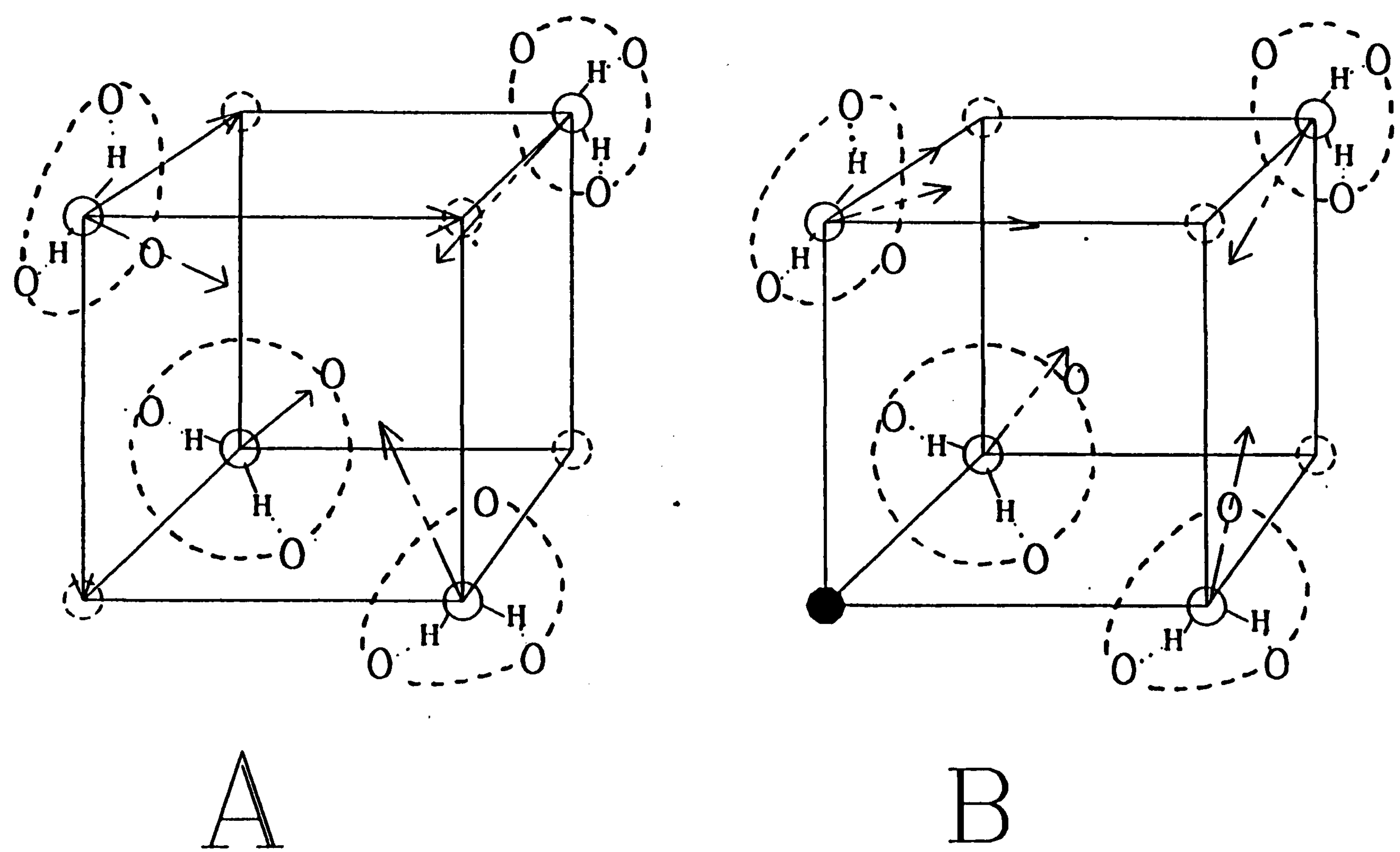

F3

F4

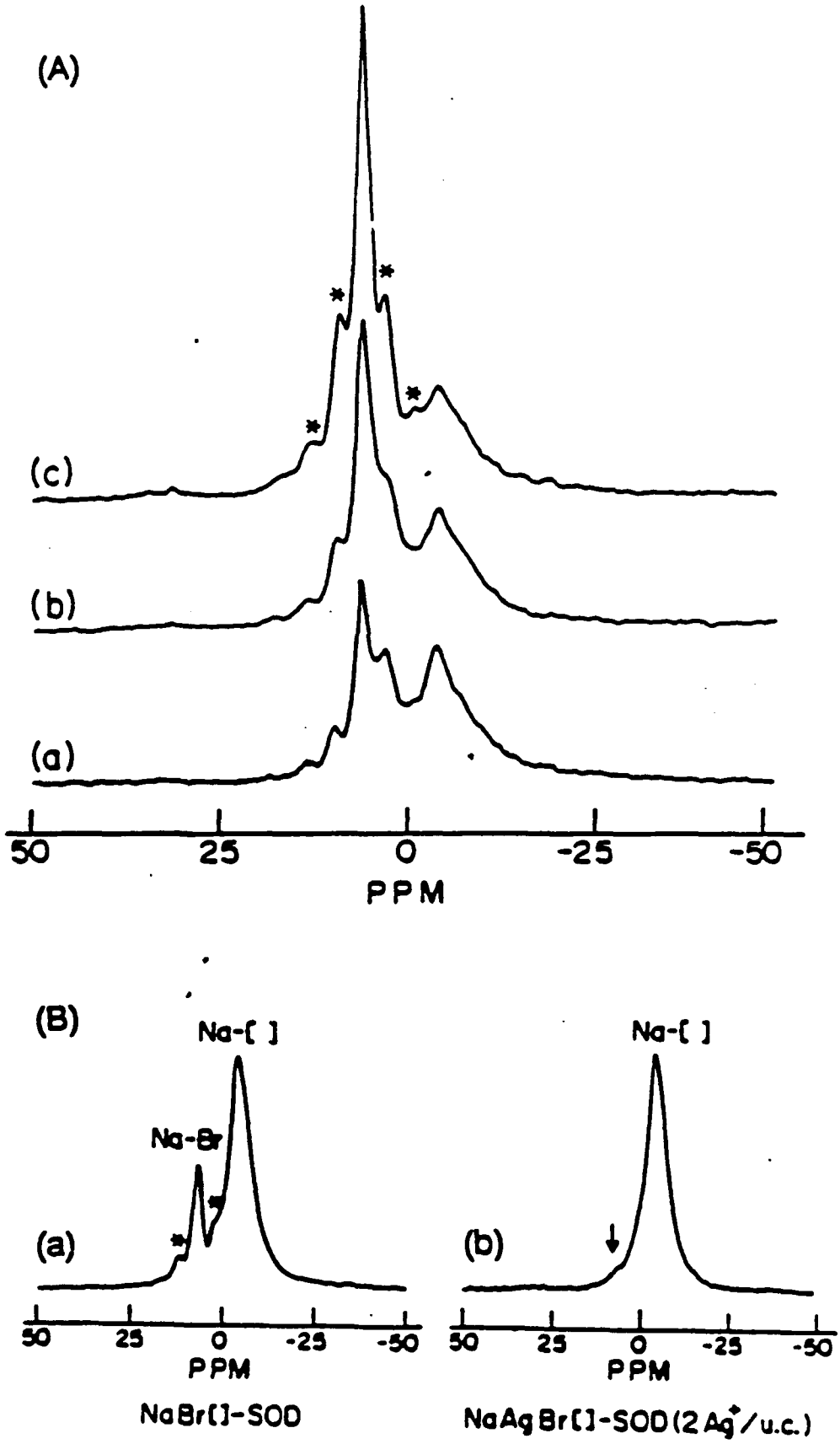
(A)
(c)
(b)
(a)
50
25
0
-25
-50
PPM
(B)
Na-[ ]
Na-Br
(a)
Na-[ ]
(b)
50
25
0
-25
-50
PPM
50
25
0
-25
-50
PPM
NaBr[]-SOD
NaAgBr[]-SOD(2 Ag+/u.c.)

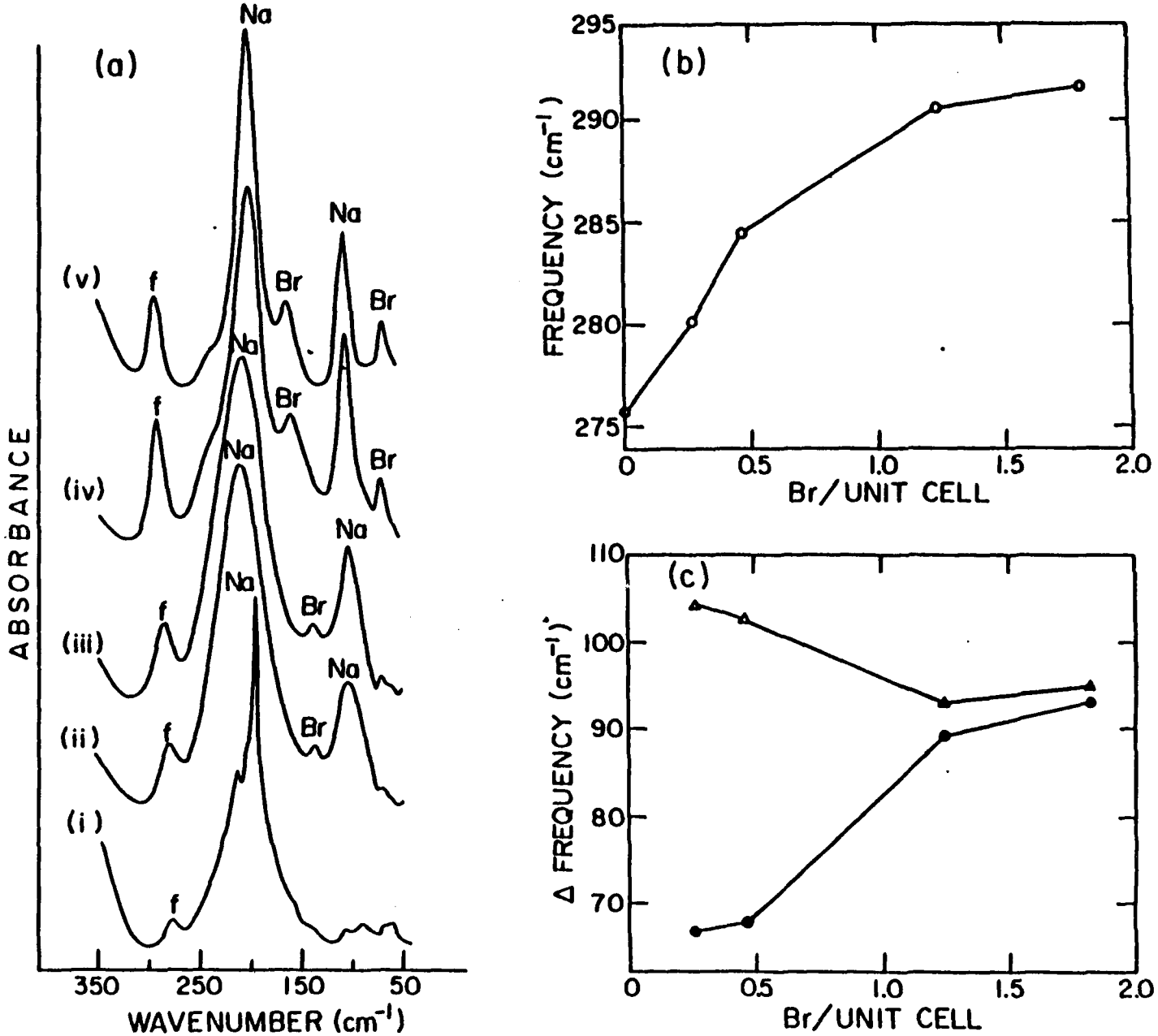
(a)
Na
f
Br
(v)
(iv)
(iii)
(ii)
(i)
ABSORBANCE
350
250
150
50
WAVENUMBER (cm⁻¹)
(b)
295
290
285
280
275
FREQUENCY (cm⁻¹)
0
0.5
1.0
1.5
2.0
Br/UNIT CELL
(c)
110
100
90
80
70
Δ FREQUENCY (cm⁻¹)
0
0.5
1.0
1.5
2.0
Br/UNIT CELL

F6

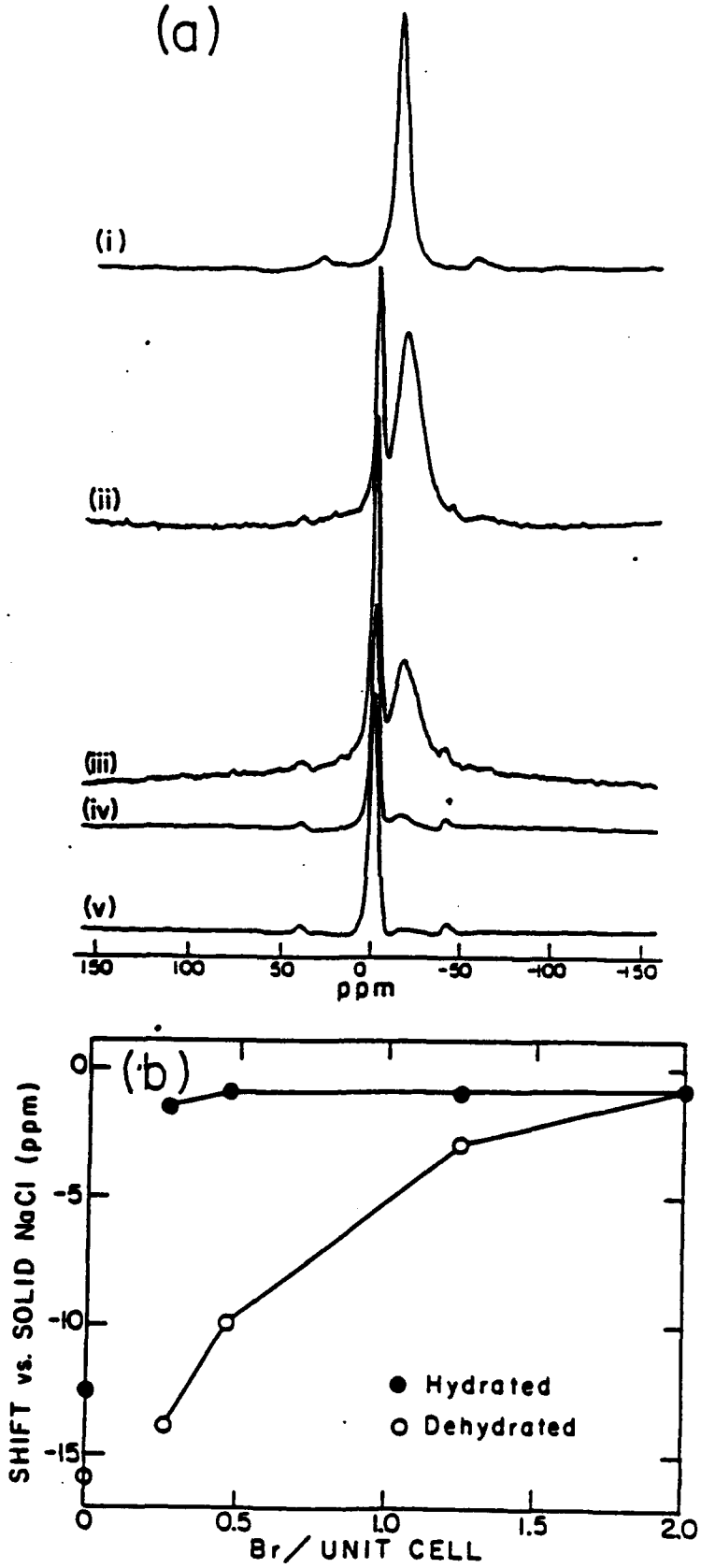
(a)
(i)
(ii)
(iii)
(iv)
(v)
150
100
50
0
-50
-100
-150
ppm
(b)
SHIFT vs. SOLID NaCl (ppm)
0
-5
-10
-15
Hydrated
Dehydrated
0
0.5
1.0
1.5
2.0
Br/ UNIT CELL

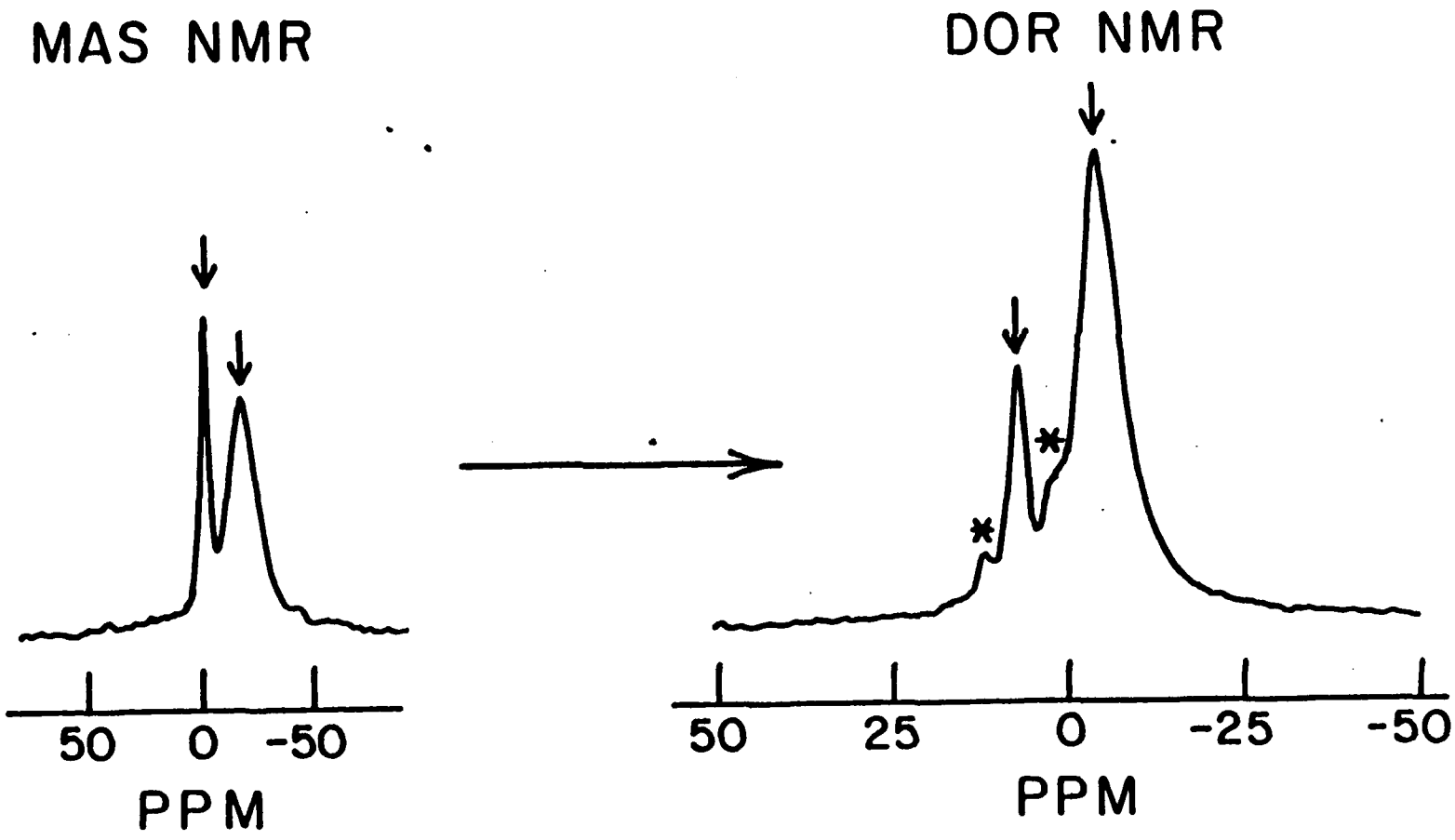
MAS NMR
DOR NMR
50
0
-50
PPM
50
25
0
-25
-50
PPM

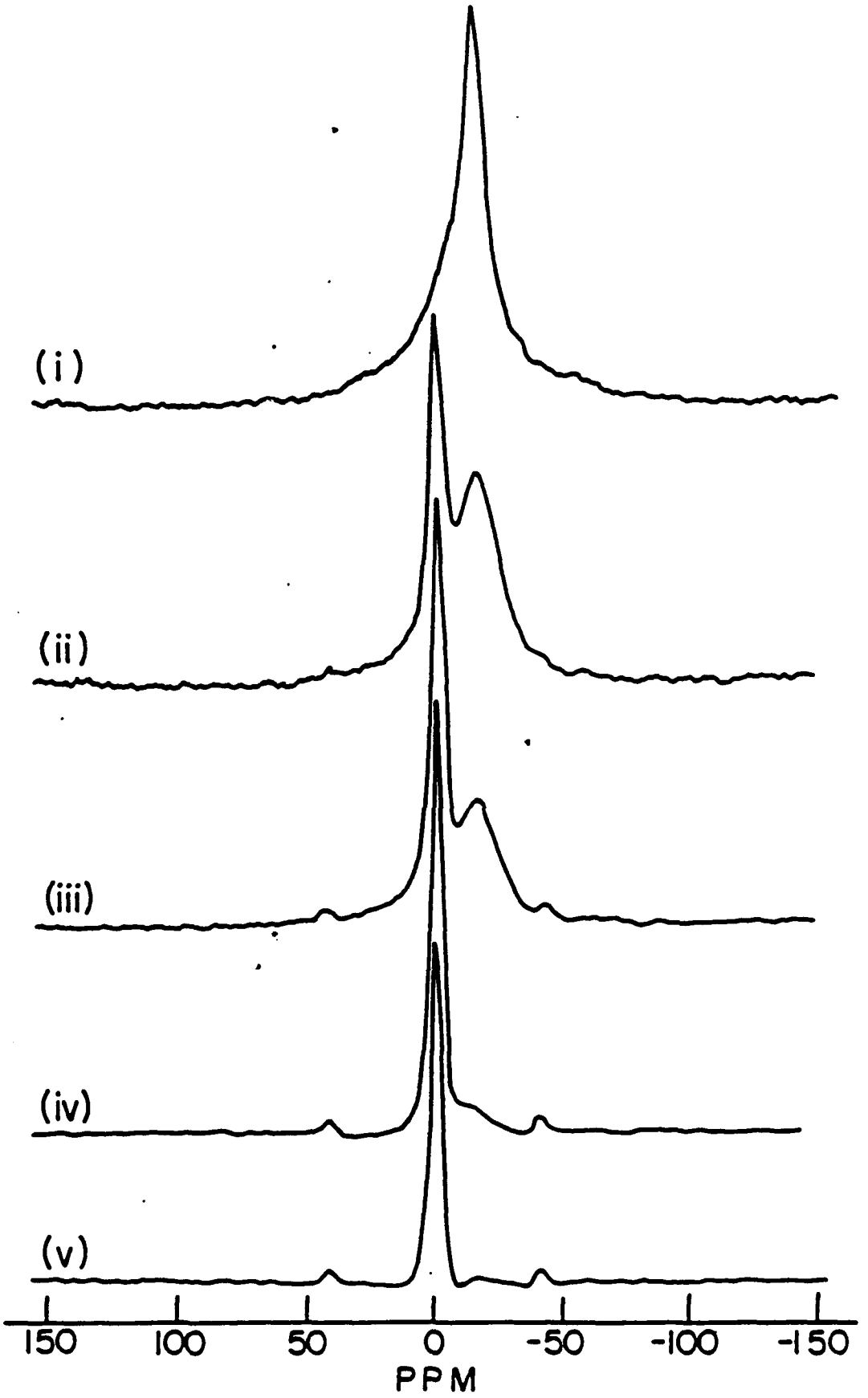
(i)
(ii)
(iii)
(iv)
(v)
150
100
50
0
-50
-100
-150
PPM

F9

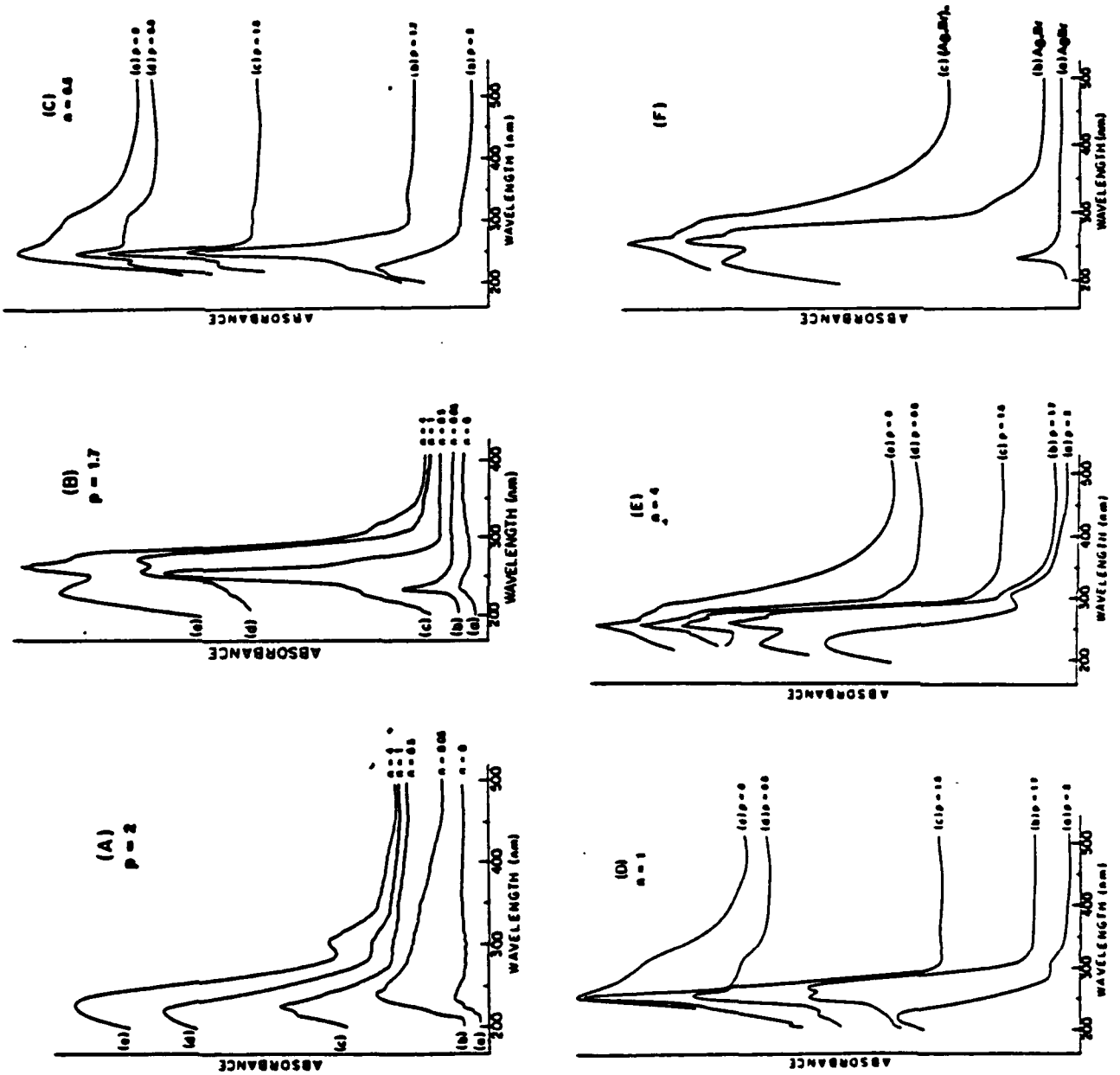

F10

Ag4Cl-SOD
Small Ag4+2 Cluster
Ag4-SOD
Ag3-SOD
NaAg2-SOD
Na2Ag-SOD
Na3-SOD
Na4Cl-SOD
Al3s,Al3p
Si3s,Si3p
Si3s,Si3p,Na3s
Cl3p,Ag5s,Ag5p,Ag4d
Cl3p
O2p
Ag5s, Ag5p
Ag5s,
Ag4d
Ag5p
Ag5sp,4d
Ag4d,5p
Ag4d,5s

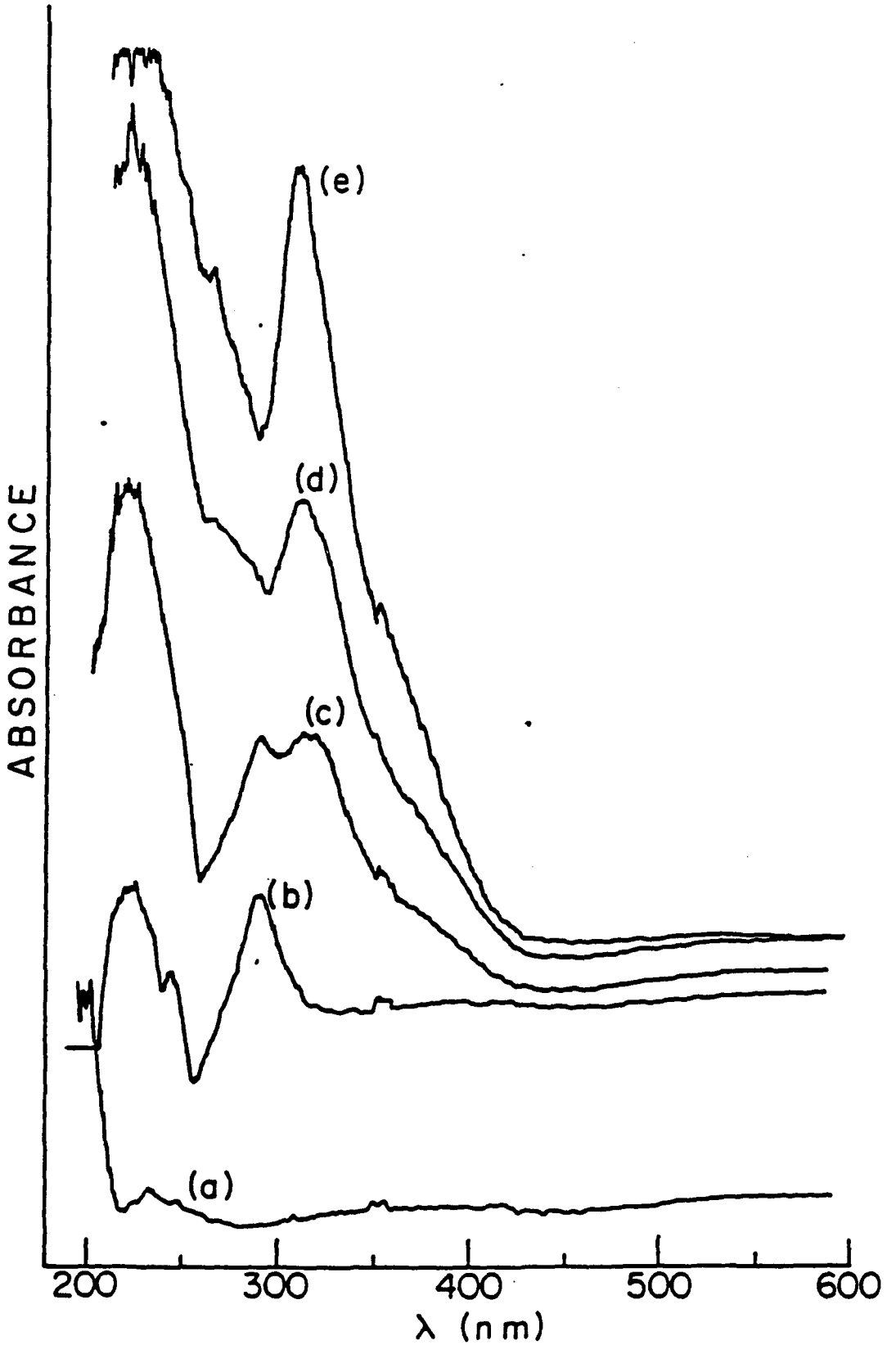
ABSORBANCE
(e)
(d)
(c)
(b)
(a)
200
300
400
500
600
λ (nm)

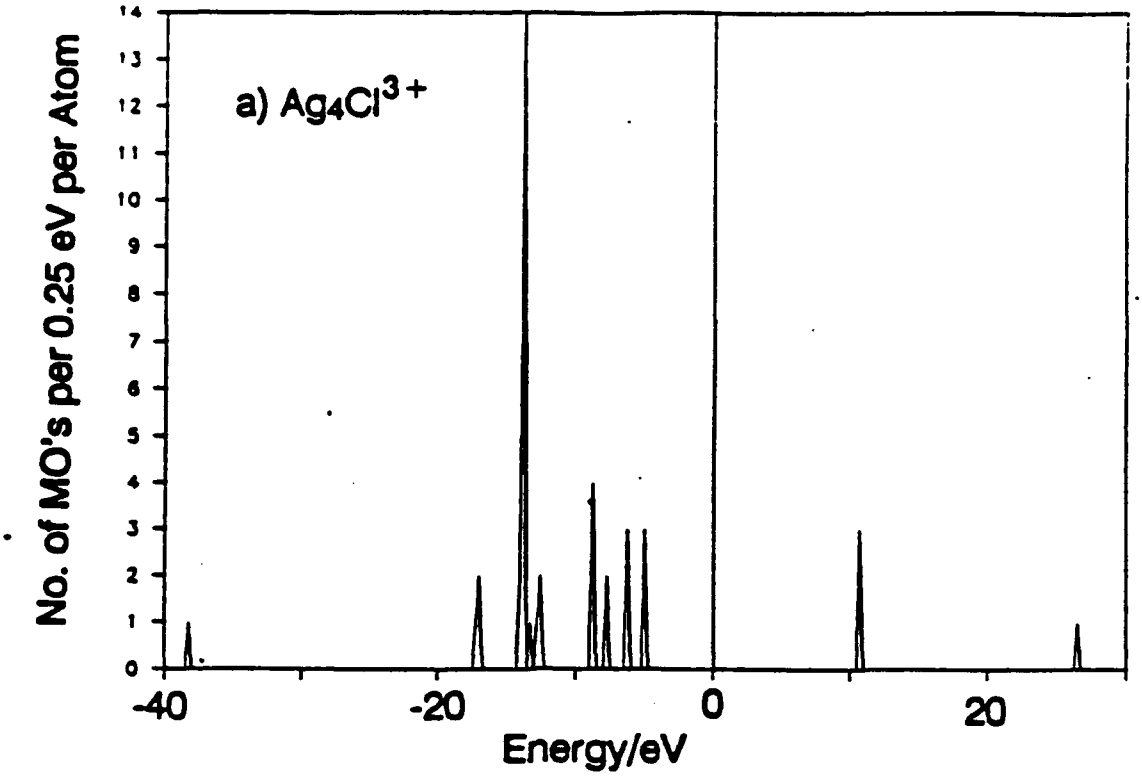
a) Ag_4Cl^{3+}
No. of MO's per 0.25 eV per Atom
Energy/eV
-40
-20
0
20

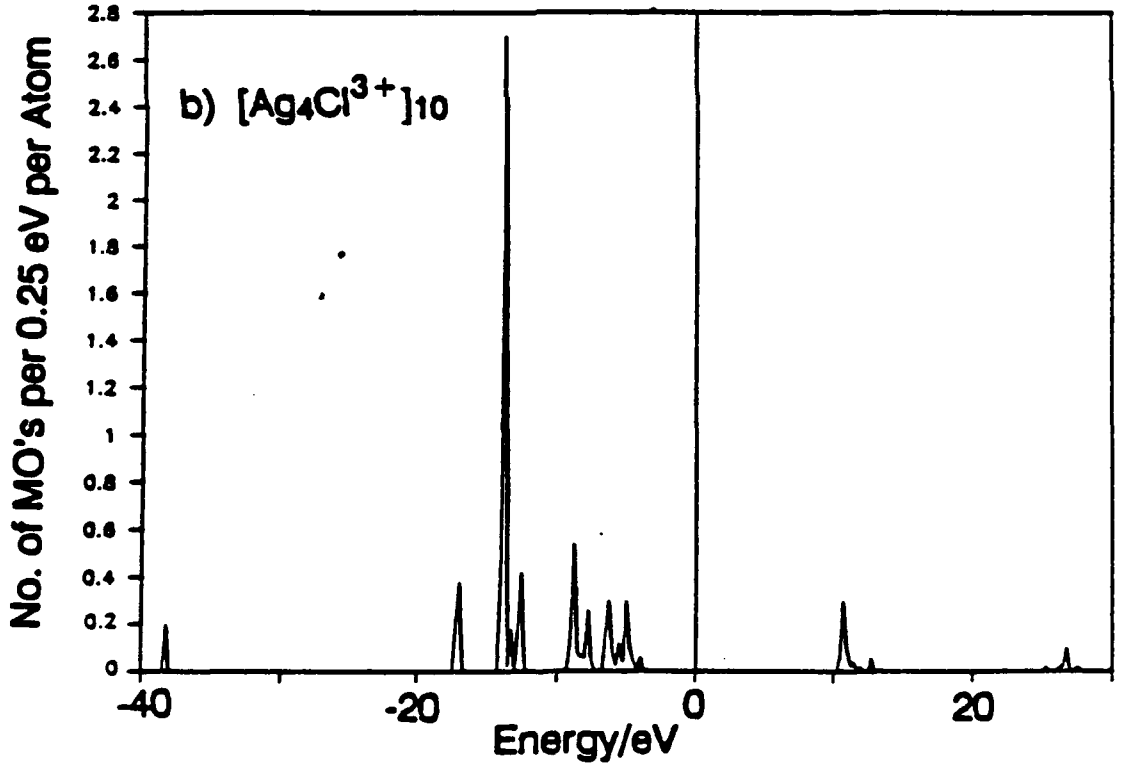
b) $[Ag_4Cl^{3+}]_{10}$
No. of MO's per 0.25 eV per Atom
Energy/eV
-40
-20
0
20

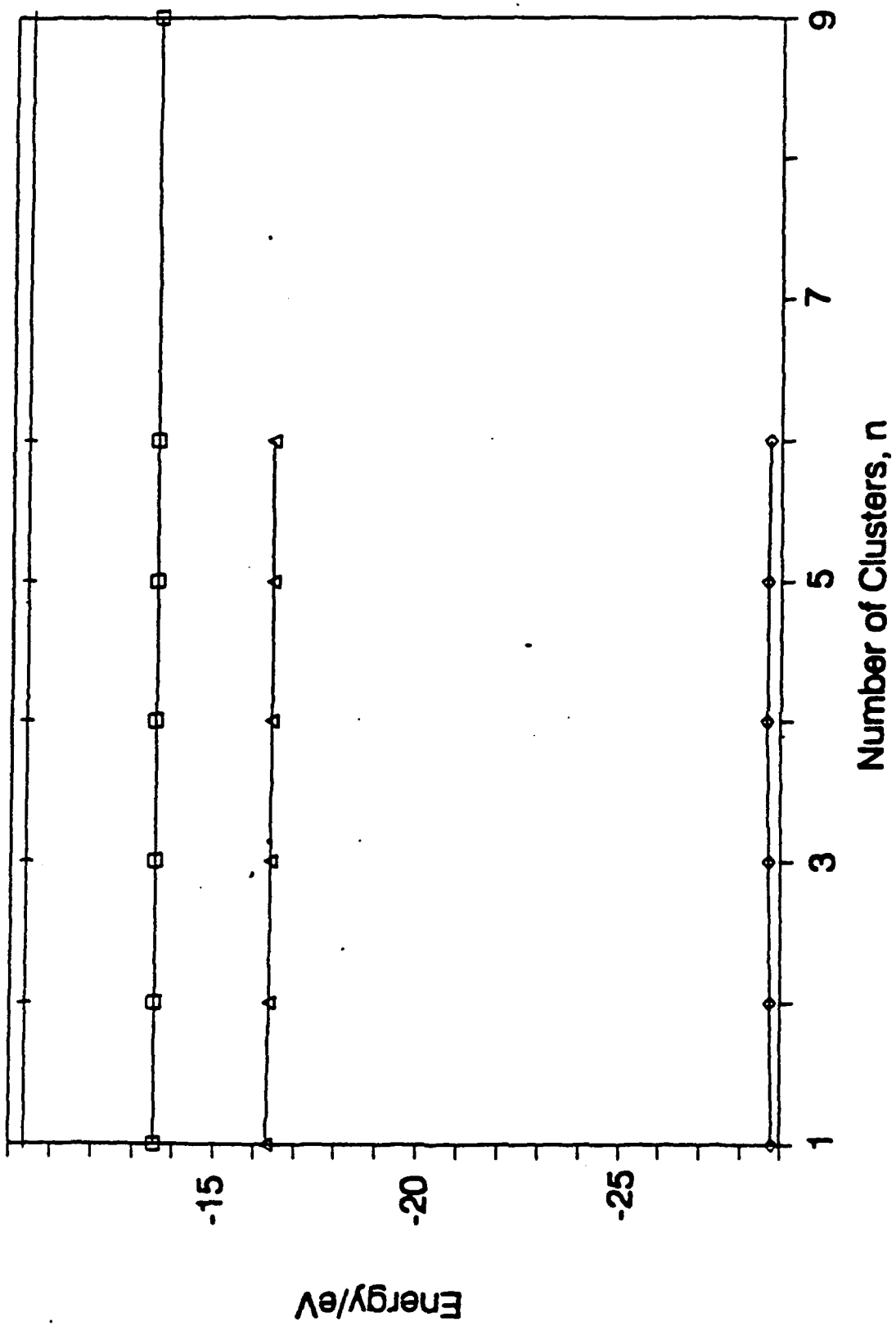
Energy/eV
-15
-20
-25
1
3
5
7
9
Number of Clusters, n

F14

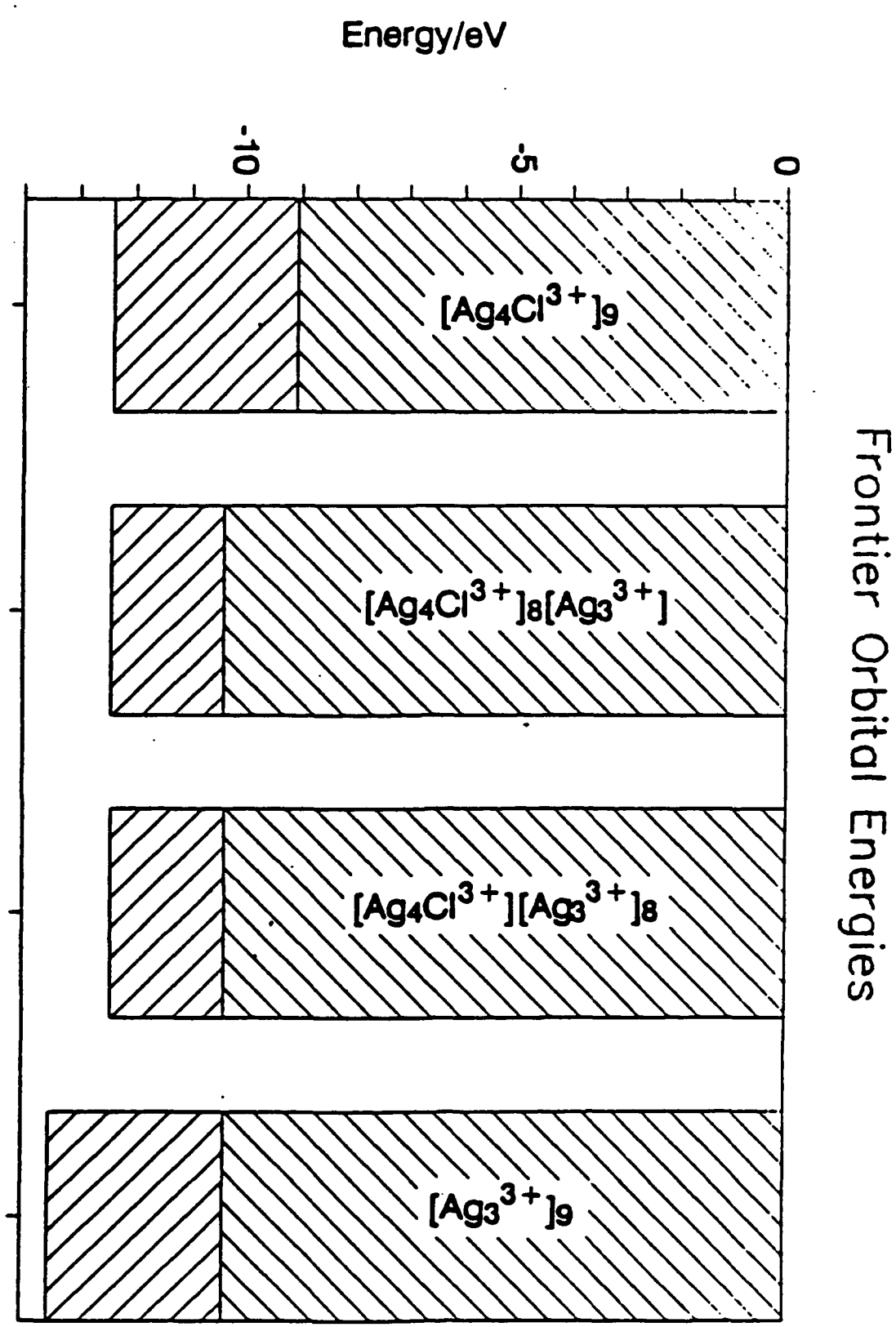
Energy/eV
-10
-5
0
$[Ag_4Cl^{3+}]_9$
$[Ag_4Cl^{3+}]_8[Ag_3^{3+}]$
$[Ag_4Cl^{3+}][Ag_3^{3+}]_8$
$[Ag_3^{3+}]_9$
Frontier Orbital Energies

TECHNICAL REPORT DISTRIBUTION LIST - GENERAL

Office of Naval Research (2)*
Chemistry Division, Code 1113
800 North Quincy Street
Arlington, Virginia 22217-5000

Dr. James S. Murday (1)
Chemistry Division, Code 6100
Naval Research Laboratory
Washington, D.C. 20375-5000

Dr. Robert Green, Director (1)
Chemistry Division, Code 385
Naval Air Weapons Center
Weapons Division
China Lake, CA 93555-6001

Dr. Elek Lindner (1)
Naval Command, Control and Ocean
Surveillance Center
RDT&E Division
San Diego, CA 92152-5000

Dr. Bernard E. Douda (1)
Crane Division
Naval Surface Warfare Center
Crane, Indiana 47522-5000

Dr. Richard W. Drisko (1)
Naval Civil Engineering
Laboratory
Code L52
Port Hueneme, CA 93043

Dr. Harold H. Singerman (1)
Naval Surface Warfare Center
Carderock Division Detachment
Annapolis, MD 21402-1198

Dr. Eugene C. Fischer (1)
Code 2840
Naval Surface Warfare Center
Carderock Division Detachment
Annapolis, MD 21402-1198

Defense Technical Information
Center (2)
Building 5, Cameron Station
Alexandria, VA 22314

* Number of copies to forward